Abstract

PADGETT, DAVID ALAN. Nullcline Analysis as a Tethered Satellite Mission Design Tool (Under the direction of Dr. Andre P. Mazzoleni)

Tethered satellite systems have be-en proposed for many space mission applications due to the useful dynamics that can be generated in such systems. For instance, tethered satellite systems can be used to increase the orbital radius of low Earth orbit payloads using angular momentum transfer; another tethered satellite system proposal involves the use of a variable length, spinning tethered system to produce specific levels of artificial gravity in low Earth orbit. Increasing interest in tethered satellite systems necessitates a fundamental understanding of the dynamics of such systems. An analytic method of qualitatively describing the possible dynamics of a tethered satellite system is presented. This analysis is centered on the study of the sets of states at which at least one of the nondimensional time derivatives of the state variables is zero; these sets are known as the nullclines of a system and they bound regions of the phase plane in which tethered satellite behavior is similar. The qualitative analysis of the nullclines provides an explanation for, and suggests the controllability of, many types of tethered satellite behavior. A Tethered Artificial Gravity (TAG) satellite system is used as a canonical tethered system and the results derived are applied to this system. The utility of the described analytical method is demonstrated by using the method to characterize two different tethered satellite missions.

NULLCLINE ANALYSIS AS A TETHERED SATELLITE MISSION DESIGN TOOL

BY

David Alan Padgett

A THESIS SUBMITTED TO THE GRADUATE FACULTY OF

NORTH CAROLINA STATE UNIVERSITY

IN PARTIAL FULFILLMENT OF THE

REQUIREMENTS FOR THE DEGREE OF

MASTER OF SCIENCE

AEROSPACE ENGINEERING

RALEIGH

January 2006

APPROVED BY:

_____

CHAIR OF ADVISORY COMMITTEE

_____

_____

Biography

David Alan Padgett was born to Kathy and Glenn Padgett in Columbia, South Carolina on March 1, 1982. He lived in West Columbia and was educated in the Lexington School District 1 system until the 10^{th} grade. In 1998 he applied and was accepted into the South Carolina Governor's School for Science and Mathematics. Upon graduation, he attended Auburn University where, in 2004, he recieved a Bachelor of Science degree with a Physics major and a Bachelor of Aerospace Engineering degree. In 2004 he began graduate studies at North Carolina State University. Upon the completion of his Master of Science (Aerospace Engineering) degree, he plans to pursue his Ph.D. (Aerospace Engineering) at North Carolina State University.

Acknowledgments

A long succession of people have helped me get to the milestone that this thesis represents, beginning with my parents. Without their love, support, and high expectations over the years, I would not have made bettering myself through education a high priority and would certainly not be where I am today. I would also like to thank the teachers at the South Carolina Governor's School for Science and Mathematics for giving me the tools necessary to carve out my academic path in college. Specifically, Dr. Clyde Smith, Dr. Mark Godwin, Mrs. Elizabeth Bunn, Mr. Arthur Squillante, Mr. Fred Lynn, Mrs. Janet Rutherford, and the Drs. Long had a large effect on formation of my academic personality while at Governor's School.

Several professors at Auburn University guided me during my four years of undergraduate study. Dr. Jack Brown and Dr. J.P. Holmes of the Mathematics Department were clear and patient teachers. Drs. Watson, Swanson, Fukai, Dong, and Thomas of the Physics Department all helped me successfully navigate the physics curriculum at Auburn. From the Department of Aerospace Engineering, Drs. Jenkins, Burkhalter, Foster, Hartfield, Cochran, and Gross as well as Col. Voss all helped to nurture my love of things that fly. I would also like to specifically thank Dr. Christopher Roy for pointing me toward North Carolina State, Dr. David Cicci for recommending me to Dr. Andre Mazzoleni of North Carolina State, and Dr. Ron Barrett for taking me under his wing during my first years at Auburn.

I would like to thank the members of my committee, Dr. Gregory Buckner and Dr. James Selgrade whose comments and advise helped me in the completion of this

thesis. Finally, I would like to thank Dr. Andre Mazzoleni of North Carolina State University without whose patience and guidance this milestone would not have been reached.

Table of Contents

List of Tables

List of Figures

Chapter 1

Literature Review and State of the Art

1.1 A Historical Overview of Tethers in Space

1.1.1 Long Structures in Space: Theoretical Studies

The first recorded investigation of a long body designed to facilitate access to space was performed by Tsiolkovskii before the turn of the 20th century. The device Tsiolkovskii described was a tower built from the earth to space. Tsiolkovskii described the variation of the force of gravity at points along the length of the tower and this design can be described as the first space elevator concept[1]. The literature concerning tethered satellites and the behavior of long bodies in the space environment is very scarce in the time between the investigation of Tsiolkovskii and the late 1950s. With the launch of Sputnik in 1957, research into many different space activities increased and research into tethered satellite motion was no exception. In 1958 J. L. Synge read

a paper before the Royal Irish Academy's Mathematics and Physical Science section concerning the behavior of a pendulum attached to a tethered satellite. Synge used lagrangian and newtonian analysis to describe the general behavior of a pendulum and identifies two configurations (the vertical configurations of a pendulum) which are stable under the gravity gradient[2]. Research into tethered satellites as space elevators was also generated after the launch of Sputnik. Bekey describes Artsutanov's space-anchored elevator as an extension of Tsiolkovskii's earth-anchored idea. Artsutanov's design involves a satellite whose center of mass is held at a geosynchronous orbit. The satellite would be capable of deploying a tether down to the surface of the earth and a ballast mass away from the surface of the earth in order to ensure that the center of mass of the system would remain in an equatorial orbit. Artsutanov described this design in 1960.

The first in-situ experimental investigation of the behavior of tethered bodies in space was carried out by NASA as part of the Gemini missions. During Gemini XI and XII, the Gemini spacecraft was tethered to the accompanying Agena spacecraft and a variety of experiments were performed[3, 4]. The initial interest in these experiments was to investigate the utility of a tether as a sort of life line or buoy for astronauts separated from their spacecraft[5]. The experiments carried out by the Gemini missions, however, were not relegated only to the use of tethers as a lifeline.

In fact, the Gemini astronauts were able to observe both gravity gradient stabilization and artificial gravity as a result of the tether experiments performed[3, 4]. The observation of these effects so early in the space program is significant because both artificial gravity and gravity gradient stabilization are results of tethered satellite motion that continue to be central to tethered satellite mission concepts.

1.1.2 Tethered Satellite Applications and Experimental Research

The tethered satellite research in the 1970s and 1980s saw a shift from basic research regarding tethered satellite dynamics to a mix between basic research and the identification and investigation of potential uses of tethered satellites. The first practical use of space tethers seriously investigated was as a class of space sensor. Colombo proposed using tethered satellites as sensors to measure both the magnetic field surrounding the Earth and the gravitational gradient at different positions around the earth[6]. Grossi investigated the use of tethered satellites as orbiting ULF/ELF antenna[7] while Colombo, Dobrowolny, and Grossi investigated the electrodynamic interaction between a metallic tether and the plasma environment and magnetic field found in low earth orbit[8]. During the period in which the Space Shuttle was being designed, Colombo proposed a tethered sensor array for use on the space shuttle. Such an array would have the ability to extend the range of environments the shuttle

could study by providing a probe to travel into the lower atmosphere of the Earth[6]. While this did not become a permanent part of the Space Shuttle, tethered satellite missions have flown on the Shuttle on a single-mission basis.

The 1990s saw the first space tether missions flown since the Gemini missions of the 1960s. The first tethered satellite mission to be flown in the 1990s was the Tethered Satellite System (TSS) which was flown on board the Space Shuttle in 1992. A jam in the reeling mechanism prevented the TSS from reaching its full mission lifetime, but much useful data was gathered in the time that the TSS mission was operational. A reflight of the TSS mission in 1996 was successful in unreeling the tether and the mission ended when the tether was severed by an unexpected electrical spark. Despite the fact that neither TSS mission reached its full design lifetime, the missions resulted in the acquisition of valuable data regarding the dynamics of tethered systems as well as the interaction of tethered systems with the space environment. The Small Expendable Deployer System missions (SEDS-1 and SEDS-2) were flown in 1993 and 1994 respectively using Delta II launch vehicles. SEDS-1 demonstrated the need for tether reel-out control as the end body recoiled after a failure in the tether braking system. This failure was not reproduced on the SEDS-2 mission and each SEDS mission was able to gather valuable data regarding the dynamics of tethered satellites in orbit. Perhaps the most successful tethered satellite mission is the TiPS (Tether Physics and Survivability) mission flown by the Naval Research Laboratory in 1996.

The TiPS mission features a highly survivable tether and as of this writing is still in orbit and visible with the use of a pair of binoculars. The TiPS mission was followed by the Advanced Tether Experiment (ATEX). This experiment was also funded by the Naval Research Laboratory through the National Reconnaissance Office and was aborted because the tether libration (pendular motion) about the center of mass reached unsafe levels.

1.2 A Review of Tethered Satellite Dynamics and Applications Literature

Tethered satellites are capable of accomplishing many different types of missions that cannot be accomplished with typical satellites because of the dynamics that are introduced to a tethered system by the tension forces traveling through the tether. The dynamics that are introduced by the tension forces have been studied extensively beginning in the 1950s with the paper of Synge previously mentioned[2]. In the 1960s, the dynamics of tethered satellite systems in the context of rotating space stations were studied by Chobotov[9, 10], Tai and Loh[11], Pengelley[12], Nixon[13], and Austin[14]. Much basic research into the dynamics of tethered satellite systems (also known as cable-connected systems in the 1960s and 1970s) was conducted in the Soviet Union by Beletsky (Beletskii)[15], Singh[16] and Efimenko[17]. Further

early research into the dynamics of tethered satellites was performed by Bainum and Evans[18, 19] while Crist and Eisley[20] and Targoff[21] studied the vibrational modes experienced by tethered satellite systems on orbit.

With the increase in knowledge concerning the dynamics of tethered satellite systems through the 1960s and 1970s, researchers began to focus on application based research rather than focusing solely on basic research. These applications include systems using the Skyhook orbital injection paradigm[22, 23] such as the Momentum Exchange and Electrodynamic Reboost vehicle (MXER). Penzo suggests using a tether to augment course changes provided by the gravitational attraction of asteroids[24]. Bekey describes Grossi's research into the use of tethered satellite systems as antennas and Colombo's concepts of tethered satellites as orbiting magnetometers and gravitometers[1]. Gravitational investigation devices have also been studied by Lorenzini[25]. Dobrowolny, Colombo, and Grossi describe methods of using the interaction between current-carrying satellites and the electromagnetic structure of near-Earth space[8]. Vallerani and Bevilacqua suggest that tethered satellites could be used to facilitate rendezvous between two co-orbiting bodies by eliminating the need for chemical propellants to make such rendezvous possible[26]. Furthermore, Vallerani and Bevilacqua suggest that simple tethered satellites could be used as orbiting atmospheric testing stations capable of gathering important aerothermodynamic data[26]. The utility of tethered satellites in gathering planetary atmospheric

data has also been investigated by Hurlbut[27] and Lorenzini[28]. A tethered array as the basis of the Terrestrial Planet Finder has been studied[29] and the dynamics of tethered sections of larger, rigid spacecraft have been investigated[30, 31]. A variety of other uses are presented in the Tethers in Space Handbook of Cosmo and Lorenzini[32].

Chapter 2

Derivation of the Equations of Motion

2.1 Vector Notation

2.1.1 Vectors and Reference Frames

Given two distinct sets of mutually perpendicular unit vectors $\mathbf{A} = \{\hat{\mathbf{a}}_\mathbf{1}, \hat{\mathbf{a}}_\mathbf{2}, \hat{\mathbf{a}}_\mathbf{3}\}$ and $\mathbf{B} = \{\hat{\mathbf{b}}_\mathbf{1}, \hat{\mathbf{b}}_\mathbf{2}, \hat{\mathbf{b}}_\mathbf{3}\}$, the vector $\vec{r}_{P/Q}$ describing the position of the point P with respect to the point Q can be written in the $\mathbf{A}$ reference frame as

$$\vec{r}_{P/Q} = \alpha_1 \hat{a}_1 + \alpha_2 \hat{a}_2 + \alpha_3 \hat{a}_3 \tag{2.1}$$

The same vector can be written in the $\mathbf{B}$ reference frame as

$$\vec{r}_{P/Q} = \beta_1 \hat{b}_1 + \beta_2 \hat{b}_2 + \beta_3 \hat{b}_3 \tag{2.2}$$

The notation $\{\vec{r}_{P/Q}\}_{\mathbf{A}}$ will denote the components of the vector $\vec{r}_{P/Q}$ in the **A** frame written as a column vector. Therefore,

$$\{\vec{r}_{P/Q}\}_{\mathbf{A}} \equiv \begin{bmatrix} \alpha_1 \\ \alpha_2 \\ \alpha_3 \end{bmatrix} \tag{2.3}$$

and similarly

$$\{\vec{r}_{P/Q}\}_{\mathbf{B}} \equiv \begin{bmatrix} \beta_1 \\ \beta_2 \\ \beta_3 \end{bmatrix} \tag{2.4}$$

The column vector $\{\vec{r}_{P/Q}\}_{\mathbf{A}}$ can be related to $\{\vec{r}_{P/Q}\}_{\mathbf{B}}$ via the formula

$$\{\vec{r}_{P/Q}\}_{\mathbf{A}} = {}^{\mathbf{A}}[C]^{\mathbf{B}}\{\vec{r}_{P/Q}\}_{\mathbf{B}} \tag{2.5}$$

where ${}^{\mathbf{A}}[C]^{\mathbf{B}}$ is the direction cosine matrix which is defined to be

$${}^{\mathbf{A}}[C]^{\mathbf{B}} \equiv \begin{bmatrix} c_{11} & c_{12} & c_{13} \\ c_{21} & c_{22} & c_{23} \\ c_{31} & c_{32} & c_{33} \end{bmatrix} \tag{2.6}$$

where

$$c_{ij} = \hat{a}_i \cdot \hat{b}_i \tag{2.7}$$

2.1.2 Vector Differentiation

The time rate of change of a vector (i.e., the derivative of a vector) must be expressed with respect to a specific reference frame. A superscript preceding the differentiation operator $\frac{d}{dt}$ denotes the frame with respect to which the vector derivative is taken. The time rate of change of the vector $\vec{r}_{P/Q}$ with respect to the **A** frame can be expressed as

$$\frac{^{\mathbf{A}}d\vec{r}_{P/Q}}{dt} = \dot{\alpha}_1\hat{a}_1 + \dot{\alpha}_2\hat{a}_2 + \dot{\alpha}_3\hat{a}_3 \tag{2.8}$$

and the time rate of change of $\vec{r}_{P/Q}$ with respect to the **B** frame can be expressed as

$$\frac{^{\mathbf{B}}d\vec{r}_{P/Q}}{dt} = \dot{\beta}_1\hat{b}_1 + \dot{\beta}_2\hat{b}_2 + \dot{\beta}_3\hat{b}_3 \tag{2.9}$$

While they both represent a time rate of change of $\vec{r}_{P/Q}$, the quantities $\frac{^{\mathbf{B}}d\vec{r}_{P/Q}}{dt}$ and $\frac{^{\mathbf{A}}d\vec{r}_{P/Q}}{dt}$ are fundamentally different because they represent the time rate of change of $\vec{r}_{P/Q}$ with respect to different reference frames. The derivatives of a vector with respect to different coordinate systems can be related to each other using the transport theorem (c.f. Kane[33]). The transport theorem states that

$$\frac{^{\mathbf{A}}d\vec{r}_{P/Q}}{dt} = \frac{^{\mathbf{B}}d\vec{r}_{P/Q}}{dt} + {}^{\mathbf{A}}\vec{\omega}^{\mathbf{B}} \times \vec{r}_{P/Q} \tag{2.10}$$

where ${}^{\mathbf{A}}\vec{\omega}^{\mathbf{B}}$ is the angular velocity of the **B** reference frame with respect to the **A** reference frame. For the given sets of unit vectors **A** and **B**, the angular velocity of

B with respect to **A** is defined as (c.f. Kane[33])

$$ {}^{\mathbf{A}}\vec{\omega}^{\mathbf{B}} = \hat{b}_1 \left(\frac{{}^{A}d\hat{b}_2}{dt} \cdot \hat{b}_3 \right) + \hat{b}_2 \left(\frac{{}^{A}d\hat{b}_3}{dt} \cdot \hat{b}_1 \right) + \hat{b}_3 \left(\frac{{}^{A}d\hat{b}_1}{dt} \cdot \hat{b}_2 \right) \tag{2.11} $$

Because velocity and acceleration are fundamental quantities in the study of dynamics, the vector $\vec{v}$ and the vector $\vec{a}$ along with preceding superscripts are reserved to express velocity and acceleration respectively. By definition, the time rate of change of $\vec{r}_{P/Q}$ (i.e., the velocity of point P with respect to point Q) with respect to the **A** reference frame is expressed

$$ {}^{\mathbf{A}}\vec{v}_{P/Q} \equiv \frac{{}^{\mathbf{A}}d\vec{r}_{P/Q}}{dt} \tag{2.12} $$

and the time rate of change of ${}^{A}\vec{v}_{P/Q}$ (i.e., the acceleration of point P with respect to point Q) with respect to the **A** reference frame is expressed

$$ {}^{\mathbf{A}}\vec{a}_{P/Q} \equiv \frac{{}^{\mathbf{A}}d\,{}^{\mathbf{A}}\vec{v}_{P/Q}}{dt} = \frac{{}^{\mathbf{A}}d^2\vec{r}_{P/Q}}{dt^2} \tag{2.13} $$

Using the definition of acceleration and velocity, the transport theorem implies that

$$ {}^{A}\vec{v}_{P/Q} = {}^{\mathbf{B}}\vec{v}_{P/Q} + {}^{\mathbf{A}}\vec{\omega}^{\mathbf{B}} \times \vec{r}_{P/Q} \tag{2.14} $$

and

$$ {}^{A}\vec{a}_{P/Q} = {}^{B}\vec{a}_{P/Q} + {}^{\mathbf{A}}\vec{\alpha}^{\mathbf{B}} \times \vec{r}_{P/Q} + 2\,{}^{\mathbf{A}}\vec{\omega}^{\mathbf{B}} \times \vec{v}_{P/Q} + {}^{\mathbf{A}}\vec{\omega}^{\mathbf{B}} \times {}^{\mathbf{A}}\vec{\omega}^{\mathbf{B}} \times \vec{r}_{P/Q} \tag{2.15} $$

where

$$ {}^{\mathbf{A}}\vec{\alpha}^{\mathbf{B}} \equiv \frac{{}^{\mathbf{A}}d\,{}^{\mathbf{A}}\vec{\omega}^{\mathbf{B}}}{dt} \tag{2.16} $$

Note that by using the transport theorem,

$$\frac{{}^{\mathbf{A}}d\,{}^{\mathbf{A}}\vec{\omega}^{\mathbf{B}}}{dt} = \frac{{}^{\mathbf{B}}d\,{}^{\mathbf{A}}\vec{\omega}^{\mathbf{B}}}{dt} + {}^{\mathbf{A}}\vec{\omega}^{\mathbf{B}} \times {}^{\mathbf{A}}\vec{\omega}^{\mathbf{B}} = \frac{{}^{\mathbf{B}}d\,{}^{\mathbf{A}}\vec{\omega}^{\mathbf{B}}}{dt} \tag{2.17}$$

so that

$${}^{\mathbf{A}}\vec{\alpha}^{\mathbf{B}} \equiv \frac{{}^{\mathbf{A}}d\,{}^{\mathbf{A}}\vec{\omega}^{\mathbf{B}}}{dt} = \frac{{}^{\mathbf{B}}d\,{}^{\mathbf{A}}\vec{\omega}^{\mathbf{B}}}{dt} \tag{2.18}$$

2.2 Definition of Coordinate Systems and Position Vectors

The coordinate systems used to derive the equations of motion are shown in Fig.2.1. The tethered satellite system **S** is aligned such that the length of tether falls along the $\hat{s_2}$ axis and the $\hat{s_2}$ coordinate of the end body m_a is positive while the $\hat{s_2}$ coordinate of the end body m_b is negative. This coordinate system moves with the tethered satellite with an instantaneous angular velocity $\dot{\theta}\hat{s_3}$. The orbital coordinate system **O** is aligned such that the vector locating the center of mass of the system is entirely along the $\hat{o_2}$ axis. The **O** reference frame moves with the orbiting center of mass with an instantaneous angular velocity $\Omega\hat{o_3}$. The earth-centered coordinate system **E** is inertial with its origin coincident with the center of the earth. The center of the Earth is labeled **C** while the center of mass of the tethered satellite is labeled **M**.

The location of the end body m_a in the **S** reference frame is given by

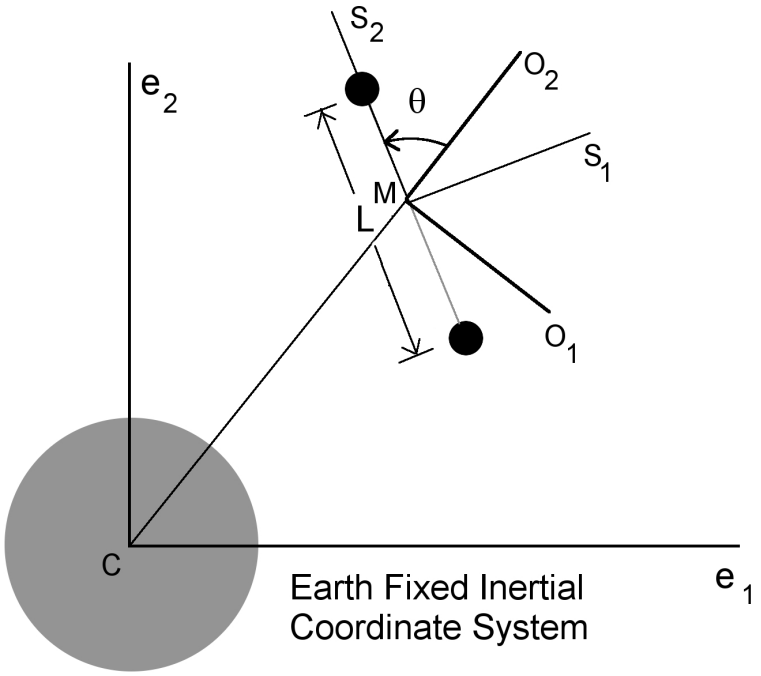

Figure 2.1: The three coordinate systems used to derive the equations of motion for a planar tethered satellite

$$\{\vec{r}_{a/M}\}_{\mathbf{S}} = \begin{bmatrix} 0 \\ l_a \\ 0 \end{bmatrix} \tag{2.19}$$

while the location of the mass m_b in the S reference frame is given by

$$\{\vec{r}_{b/M}\}_{\mathbf{S}} = \begin{bmatrix} 0 \\ -l_b \\ 0 \end{bmatrix} \tag{2.20}$$

In the **O** reference frame, the center of mass of the tethered satellite system is given by

$$\{\vec{r}_{M/C}\}_{\mathbf{O}} = \begin{bmatrix} 0 \\ r_0 \\ 0 \end{bmatrix} \tag{2.21}$$

For any vector $\vec{v}$ expressed in the O reference frame, the transformation into the S reference frame is given by

$$\{\vec{v}\}_{\mathbf{S}} = {}^{S}[C]^{O}\{\vec{v}\}_{\mathbf{O}} \tag{2.22}$$

where ${}^{S}[C]^{O}$ is given by

$$ {}^{S}[C]^{O} = \begin{bmatrix} \cos\theta & \sin\theta & 0 \\ -\sin\theta & \cos\theta & 0 \\ 0 & 0 & 1 \end{bmatrix} \tag{2.23} $$

Therefore, in the satellite reference frame S, the location of the end body m_a with respect to the center of mass of the earth C is given by

$$ \begin{aligned} \{\vec{r}_{a/\mathbf{C}}\}_{\mathbf{S}} &= \{\vec{r}_{a/M}\}_{\mathbf{S}} + {}^{S}[C]^{O}\{\vec{r}_{M/C}\}_{\mathbf{O}} \\ &= \begin{bmatrix} 0 \\ l_a \\ 0 \end{bmatrix} + \begin{bmatrix} \cos\theta & \sin\theta & 0 \\ -\sin\theta & \cos\theta & 0 \\ 0 & 0 & 1 \end{bmatrix} \begin{bmatrix} 0 \\ r_0 \\ 0 \end{bmatrix} \\ &= \begin{bmatrix} r_o \sin\theta \\ l_a + r_o \cos\theta \\ 0 \end{bmatrix} \end{aligned} \tag{2.24} $$

Likewise, the position vector of the end body m_b in the satellite coordinate system S with respect to the center of the earth is given by the vector

$$ \{\vec{r}_{b/\mathbf{C}}\}_{\mathbf{S}} = \begin{bmatrix} r_o \sin\theta \\ -l_b + r_o \cos\theta \\ 0 \end{bmatrix} \tag{2.25} $$

The derivation of the equations of motion will be carried out by applying Newton's Second Law to the vectors $\{\vec{r}_{b/\mathbf{C}}\}_{\mathbf{S}}$ and $\{\vec{r}_{a/\mathbf{C}}\}_{\mathbf{S}}$. Newton's Second Law states that, for any body of constant mass in an inertial reference frame

$$\sum \vec{F}_i = m_i \vec{a}_i \tag{2.26}$$

where $\vec{F}_i$ are the forces acting on the body, m_i is the mass of the body and a_i is the acceleration of the body in the inertial reference frame. The position vectors $\{\vec{r}_{b/\mathbf{C}}\}_{\mathbf{S}}$ and $\{\vec{r}_{a/\mathbf{C}}\}_{\mathbf{S}}$ must be differentiated twice to obtain the acceleration of the end bodies m_a and m_b. However, these vectors represent the position of the end masses in a non-inertial reference frame (the rotating frame S). The solution to this problem is to use the transport theorem[33] in order to find the inertial acceleration of vectors expressed in a non-inertial reference frame. The transport theorem for a general vector $\vec{v}$ and reference frames $\mathbf{R}$ and $\mathbf{T}$ states that

$$\frac{^R d\vec{v}}{dt} = \frac{^T d\vec{v}}{dt} + ^R\vec{\omega}^T \times \vec{v} \tag{2.27}$$

where $^R\vec{\omega}^T$ is the rotational velocity of reference frame T with respect to reference frame R. The angular velocity of the tethered satellite reference frame S with respect to the inertial reference frame E can be written

$$\begin{aligned}
\{{}^S\vec{\omega}^E\}_{\mathbf{S}} &= \{{}^S\vec{\omega}^O\}_{\mathbf{S}} + \{{}^O\vec{\omega}^E\}_{\mathbf{S}} \\
&= \begin{bmatrix} 0 \\ 0 \\ \dot{\theta} \end{bmatrix} + \begin{bmatrix} 0 \\ 0 \\ \Omega \end{bmatrix} \\
&= \begin{bmatrix} 0 \\ 0 \\ \dot{\theta} + \Omega \end{bmatrix}
\end{aligned} \tag{2.28}$$

Applying the transport theorem Eq.2.27 to the position vector of end body m_a Eq.2.24 yields

$$\begin{aligned}
\{{}^E\vec{v}_{a/\mathbf{C}}\}_{\mathbf{S}} &= \{\frac{{}^S d\vec{r}_{a/\mathbf{C}}}{dt}\}_{\mathbf{S}} + \{{}^S\vec{\omega}^E\}_{\mathbf{S}} \times \{\vec{r}_{a/\mathbf{C}}\}_{\mathbf{S}} \\
&= \begin{bmatrix} \dot{r_o}\sin\theta + r_o\dot{\theta}\cos\theta \\ \dot{l_a} + \dot{r_o}\cos\theta - r_o\dot{\theta}\sin\theta \\ 0 \end{bmatrix} + \begin{bmatrix} -(\dot{\theta}+\Omega)l_a - (\dot{\theta}+\Omega)r_o\cos\theta \\ (\dot{\theta}+\Omega)r_o\sin\theta \\ 0 \end{bmatrix} \\
&= \begin{bmatrix} \dot{r_o}\sin\theta - \dot{\theta}l_a - \Omega l_a - \Omega r_o\cos\theta \\ \dot{l_a} + \dot{r_o}\cos\theta + \Omega r_o\sin\theta \\ 0 \end{bmatrix}
\end{aligned} \tag{2.29}$$

Applying the transport theorem to this result to find the inertial acceleration of m_a expressed in the S reference frame yields

$$
\begin{aligned}
\{{}^{E}\vec{a}_{a/\mathbf{C}}\}_{\mathbf{S}} &= \{\frac{{}^{S}d\vec{v}_{a/\mathbf{C}}}{dt}\}_{\mathbf{S}} + \{{}^{S}\vec{\omega}^{E}\}_{\mathbf{S}} \times \{\vec{v}_{a/\mathbf{C}}\}_{\mathbf{S}} \\
&= \begin{bmatrix} \ddot{r_o}\sin\theta + \dot{r_o}\dot{\theta}\cos\theta - \ddot{\theta}l_a - \dot{\theta}\dot{l_a} - \dot{\Omega}l_a - \Omega\dot{l_a} - \dot{\Omega}r_o\cos\theta - \Omega\dot{r_o}\cos\theta + \Omega\dot{\theta}r_o\sin\theta \\ \ddot{l_a} + \dot{\Omega}r_o\sin\theta + \Omega\dot{r_o}\sin\theta + \Omega r_o\dot{\theta}\cos\theta + \ddot{r_o}\cos\theta - \dot{r_o}\dot{\theta}\sin\theta \\ 0 \end{bmatrix} \\
&+ \begin{bmatrix} -\Omega\dot{l_a} - \Omega^2 r_o\sin\theta - \Omega\dot{r_o}\cos\theta - \dot{\theta}\dot{l_a} - \Omega r_o\dot{\theta}\sin\theta - \dot{\theta}\dot{r_o}\cos\theta \\ -l_a\Omega^2 + \Omega\dot{r_o}\sin\theta - \Omega\dot{\theta}l_a - \Omega^2 r_o\cos\theta + \dot{\theta}\dot{r_o}\sin\theta - \dot{\theta}^2 l_a - \Omega\dot{\theta}l_a - \Omega\dot{\theta}r_o\cos\theta \\ 0 \end{bmatrix} \\
&= \begin{bmatrix} \ddot{r_o}\sin\theta - \ddot{\theta}l_a - 2\dot{\theta}\dot{l_a} - \dot{\Omega}l_a - 2\Omega\dot{l_a} - 2\Omega\dot{r_o}\cos\theta - \dot{\Omega}r_o\cos\theta - \Omega^2 r_o\sin\theta \\ \ddot{l_a} + \dot{\Omega}r_o\sin\theta + 2\Omega\dot{r_o}\sin\theta + \ddot{r_o}\cos\theta - 2\Omega\dot{\theta}l_a - \Omega^2 l_a - \Omega^2 r_o\cos\theta - \dot{\theta}^2 l_a \\ 0 \end{bmatrix}
\end{aligned} \tag{2.30}
$$

Similarly, the inertial velocity of the end body m_b can be determined by applying the transport theorem to Eq.2.25.

$$
\begin{aligned}
\{{}^E\vec{v}_{b/\mathbf{C}}\}_{\mathbf{S}} &= \{\frac{{}^S d\vec{r}_{b/\mathbf{C}}}{dt}\}_{\mathbf{S}} + \{{}^S\vec{\omega}^E\}_{\mathbf{S}} \times \{\vec{r}_{a/\mathbf{C}}\}_{\mathbf{S}} \\
&= \begin{bmatrix} \dot{r_o}\sin\theta + r_o\dot{\theta}\cos\theta \\ -\dot{l_b} + \dot{r_o}\cos\theta - r_o\dot{\theta}\sin\theta \\ 0 \end{bmatrix} + \begin{bmatrix} (\dot{\theta}+\Omega)l_b - (\dot{\theta}+\Omega)r_o\cos\theta \\ (\dot{\theta}+\Omega)r_o\sin\theta \\ 0 \end{bmatrix} \\
&= \begin{bmatrix} \dot{r_o}\sin\theta + \dot{\theta}l_b + \Omega l_b - \Omega r_o\cos\theta \\ -\dot{l_b} + \dot{r_o}\cos\theta + \Omega r_o\sin\theta \\ 0 \end{bmatrix} \qquad (2.31)
\end{aligned}
$$

Applying the transport theorem to $\{{}^E\vec{v}_{b/\mathbf{C}}\}_{\mathbf{S}}$ to obtain the inertial acceleration yields

$$
\begin{aligned}
\{{}^E\vec{a}_{b/\mathbf{C}}\}_{\mathbf{S}} &= \{\frac{{}^S d\vec{v}_{b/\mathbf{C}}}{dt}\}_{\mathbf{S}} + \{{}^S\vec{\omega}^E \times \vec{v}_{b/\mathbf{C}}\}_{\mathbf{S}} \\
&= \begin{bmatrix} \ddot{r_o}\sin\theta + \dot{r_o}\dot{\theta}\cos\theta + \dot{\Omega}l_b + \Omega\dot{l_b} + \ddot{\theta}l_b + \dot{\theta}\dot{l_b} - \dot{\Omega}r_o\cos\theta - \Omega\dot{r_o}\cos\theta + \Omega r_o\dot{\theta}\sin\theta \\ -\ddot{l_b} + \ddot{r_o}\cos\theta - \dot{r_o}\dot{\theta}\sin\theta + \dot{\Omega}r_o\sin\theta + \Omega\dot{r_o}\sin\theta + \Omega r_o\dot{\theta}\cos\theta \\ 0 \end{bmatrix} \\
&+ \begin{bmatrix} \Omega\dot{l_b} - \Omega\dot{r_o}\cos\theta - \Omega^2 r_o\sin\theta + \dot{\theta}\dot{l_b} - \dot{\theta}\dot{r_o}\cos\theta - \Omega r_o\dot{\theta}\sin\theta \\ l_b\Omega^2 + \Omega\dot{r_o}\sin\theta + \Omega\dot{\theta}l_b - \Omega^2 r_o\cos\theta + \dot{\theta}\dot{r_o}\sin\theta + \dot{\theta}^2 l_b + \Omega\dot{\theta}l_b - \Omega\dot{\theta}r_o\cos\theta \\ 0 \end{bmatrix} \\
&= \begin{bmatrix} \ddot{r_o}\sin\theta + \ddot{\theta}l_b + 2\dot{\theta}\dot{l_b} + \dot{\Omega}l_b + 2\Omega\dot{l_b} - 2\Omega\dot{r_o}\cos\theta - \dot{\Omega}r_o\cos\theta - \Omega^2 r_o\sin\theta \\ -\ddot{l_b} + \dot{\Omega}r_o\sin\theta + 2\Omega\dot{r_o}\sin\theta + \ddot{r_o}\cos\theta + 2\Omega\dot{\theta}l_b + \Omega^2 l_b - \Omega^2 r_o\cos\theta + \dot{\theta}^2 l_b \\ 0 \end{bmatrix} \qquad (2.32)
\end{aligned}
$$

2.2.1 The Sum of the Forces on Each Mass

Assume that the only forces acting on the end bodies are the gravitational force and the tension force traveling along the length of the tether. Other forces, such as high altitude atmospheric drag forces, electrodynamic forces, and radiation pressure forces will be ignored. Therefore, the sum of the forces acting on each mass is

$$\sum \vec{F} = \vec{F}_g + \vec{T} \tag{2.33}$$

where F_g is the gravitational force acting on the mass and T is the tether tension force traveling through the tether. The gravitational force acting on the mass m_a is.

$$\vec{F}_{ga} = -\frac{GMm_a}{|\vec{r}_{a/C}|^3}\vec{r}_{a/C} \tag{2.34}$$

The magnitude of the vector $\vec{r}_{a/C}$ can be determined by using the law of cosines

$$|\vec{r}_{a/C}| = \sqrt{r_o^2 + l_a^2 - 2r_o l_a \cos(\pi - \theta)} \tag{2.35}$$

Using the identity $\cos\pi - \theta = -\cos\theta$ and factoring r_o^2 from the radical gives

$$|\vec{r}_{a/C}| = r_o\sqrt{1 + \frac{l_a^2}{r_o^2} + 2\frac{l_a}{r_o}\cos\theta} \tag{2.36}$$

Evaluating the magnitude of the r_a to the -3^{rd} power yields

$$|\vec{r}_{a/C}|^{-3} = r_o^{-3}(1 + \frac{l_a^2}{r_o^2} + 2\frac{l_a}{r_o}\cos\theta)^{-\frac{3}{2}} \tag{2.37}$$

Because $\frac{l_a^2}{r_o^2} << 1$, the term will be ignored. Applying the binomial expansion to Eq.2.37 yields

$$|\vec{r}_{a/C}|^{-3} = r_o^{-3}(1 - 3\frac{l_a}{r_o}\cos\theta) \tag{2.38}$$

where terms involving $\frac{l_a^2}{r_o^2}$ of order higher than one have been approximated as zero. Therefore, Eq.2.34 becomes

$$\frac{1}{m_a}\{\vec{F}_{ga}\}_{\mathbf{S}} = -\frac{GM}{r_o^3}(1 - 3\frac{l_a}{r_o}\cos\theta)\{\vec{r}_{a/C}\}_{\mathbf{S}} \tag{2.39}$$

$$= -\Omega^2(1 - 3\frac{l_a}{r_o}\cos\theta)\begin{bmatrix} r_o\sin\theta \\ l_a + r_o\cos\theta \\ 0 \end{bmatrix} \tag{2.40}$$

The gravitational force acting on mass m_b can be determined using the same approximations

$$\vec{F}_{gb} = -\frac{GMm_b}{|\vec{r}_{b/C}|^3}\vec{r}_{b/C} \tag{2.41}$$

The magnitude $|\vec{r}_{b/C}|^{-3}$ is given by

$$|\vec{r}_{b/C}|^{-3} = (r_o^2 + l_b^2 - 2l_b r_o \cos\theta)^{-\frac{3}{2}} \tag{2.42}$$

Factoring r_o from Eq.2.42 gives

$$|\vec{r}_{b/C}|^{-3} = r_o^{-3}(1 + \frac{l_b^2}{r_o^2} - 2\frac{l_b}{r_o}\cos\theta)^{-\frac{3}{2}} \tag{2.43}$$

Because $\frac{l_b^2}{r_o^2} << 1$, Eq.2.43 can be approximated by

$$|\vec{r}_{b/C}|^{-3} = r_o^{-3}(1 - 2\frac{l_b}{r_o}\cos\theta)^{-\frac{3}{2}} \tag{2.44}$$

Using the binomial expansion and approximating higher order $\frac{l_b}{r_o}$ terms as zero gives

$$|\vec{r}_{b/C}|^{-3} = r_o^{-3}(1 + 3\frac{l_b}{r_o}\cos\theta) \tag{2.45}$$

Therefore, the gravitational force on m_b is

$$\frac{1}{m_b}\{\vec{F}_{gb}\}_{\mathbf{S}} = -\frac{GM}{r_o^3}(1 + 3\frac{l_b}{r_o}\cos\theta)\{\vec{r}_{b/C}\}_{\mathbf{S}} \tag{2.46}$$

$$= -\Omega^2(1 + 3\frac{l_b}{r_o}\cos\theta)\begin{bmatrix} r_o\sin\theta \\ -l_b + r_o\cos\theta \\ 0 \end{bmatrix} \tag{2.47}$$

The tether tension force acting on the mass m_a is

$$\{\vec{F}_{Ta}\}_{\mathbf{S}} = \begin{bmatrix} 0 \\ -T \\ 0 \end{bmatrix} \tag{2.48}$$

while the tension force acting on the mass m_b is

$$\{\vec{F}_{Tb}\}_{\mathbf{S}} = \begin{bmatrix} 0 \\ T \\ 0 \end{bmatrix} \tag{2.49}$$

2.2.2 Applying Newton's Second Law

For constant mass systems, Newton's Second Law can be rewritten as

$$\frac{1}{m_i}\sum \vec{F}_i = \vec{a}_i \tag{2.50}$$

Eq.2.50 will be applied to the tethered satellite system by subtracting ${}^{E}\vec{a}_{a/\mathbf{C}}$ from ${}^{E}\vec{a}_{b/\mathbf{C}}$ as follows

$${}^{E}\vec{a}_{b/\mathbf{C}} - {}^{E}\,\vec{a}_{a/\mathbf{C}} = \frac{1}{m_b}\vec{F}_b - \frac{1}{m_b}\vec{F}_a \tag{2.51}$$

where

$$\{^E\vec{a}_{b/\mathbf{C}}\}_\mathbf{S} - \{^E\vec{a}_{a/\mathbf{C}}\}_\mathbf{S} = \begin{bmatrix} \ddot{\theta}L + 2\dot{\theta}\dot{L} + \dot{\Omega}L + 2\Omega\dot{L} \\ -\ddot{L} + 2\Omega\dot{\theta}L + \Omega^2 L + \dot{\theta}^2 L \\ 0 \end{bmatrix} \tag{2.52}$$

and

$$\frac{1}{m_b}\{\vec{F}_b\}_\mathbf{S} - \frac{1}{m_b}\{\vec{F}_a\}_\mathbf{S} = \begin{bmatrix} -3\Omega^2 L\cos\theta\sin\theta \\ \Omega^2 L - 3\Omega^2 L\cos^2\theta - 3\Omega^2\frac{l_b^2+l_a^2}{r_o}\cos\theta + \frac{T}{m_b} + \frac{T}{m_a} \\ 0 \end{bmatrix} \tag{2.53}$$

Making the approximation that the center of mass of the tethered satellite system orbits the earth in a circular path (i.e., $\dot{\Omega} = 0$) and that $r_o >> l_b^2 + l_a^2$, and making the substitutions $\bar{m} = \frac{m_a m_b}{m_a + m_b}$ and $\cos\theta\sin\theta = \frac{1}{2}\sin 2\theta$, Eq.2.51 becomes

$$\begin{bmatrix} \ddot{\theta}L + 2\dot{\theta}\dot{L} + 2\Omega\dot{L} \\ -\ddot{L} + 2\Omega\dot{\theta}L + \Omega^2 L + \dot{\theta}^2 L \\ 0 \end{bmatrix} = \begin{bmatrix} -\frac{3}{2}\Omega^2 L\sin 2\theta \\ \Omega^2 L - 3\Omega^2 L\cos^2\theta + \frac{T}{\bar{m}} \\ 0 \end{bmatrix} \tag{2.54}$$

Taking each component separately gives the two equations of motion for a planar dumbbell satellite in their most common form

$$\ddot{\theta}L + 2\dot{\theta}\dot{L} + 2\Omega\dot{L} = -\frac{3}{2}\Omega^2\sin 2\theta$$

which implies

$$\ddot{\theta} + 2\frac{\dot{L}}{L}(\dot{\theta} + \Omega) + \frac{3}{2}\Omega^2\sin 2\theta = 0 \tag{2.55}$$

and

$$-\ddot{L} + 2\Omega\dot{\theta}L + \Omega^2 L + \dot{\theta}^2 L = \Omega^2 L - 3\Omega^2 L\cos^2\theta + \frac{T}{\bar{m}}$$

which implies

$$\ddot{L} - L(2\Omega\dot{\theta} + \dot{\theta}^2 + 3\Omega^2\cos^2\theta) = -\frac{T}{\bar{m}} \tag{2.56}$$

2.3 An Analysis of the Dimensional Equations of Motion

Eq.2.55 and Eq.2.56 are the equations of motion which model the dynamics of a two-body tethered satellite under the "Planar Dumbbell" approximations with an exponential tether reel-in control law. The tether is assumed to be massless and inextensible. The orbit of the center of mass has been assumed to be circular, making $\Omega = \sqrt{\frac{GM}{r_o}}$ a constant value. Earth has been assumed to be spherical and to have a spherically symmetric density profile. Atmospheric and radiation forces have been neglected. Furthermore, the length of the tether is assumed to be given by the control law

$$L = L_i e^{-ct} \tag{2.57}$$

where c is defined as

$$c = \frac{ln(\frac{L_i}{L_f})}{t_r} \tag{2.58}$$

and L_i is the initial tether length, L_f is the final tether length, and t_r is the amount of time required for the tether to be reeled in from L_i to L_f. The use of the tether control law Eq.2.57 gives a system of three equations

$$\begin{aligned} \ddot{L} - L(2\Omega\dot{\theta} + \dot{\theta}^2 + 3\Omega^2 L\cos^2\theta) &= -\frac{T}{\bar{m}} \\ \ddot{\theta} + 2\frac{\dot{L}}{L}(\dot{\theta} + \Omega) + \frac{3}{2}\Omega^2 \sin 2\theta &= 0 \\ L &= L_i e^{-ct} \end{aligned}$$

with three sets of unknowns: θ and its derivatives as a function of time, L and its derivatives as a function of time, and the tether tension force T as a function of time. The tether length L at any point in time is given by the tether length control law. This law can be substituted into Eq.2.55 and with an appropriate number of initial conditions, the angular position θ and velocity $\dot{\theta}$ of the tethered satellite as a function of time can be found. The tether length control law Eq.2.57 and the angular position and velocity of the tethered satellite as a function of time can then be substituted into Eq.2.56 to determine the tether tension T as a function of time. While the magnitude of the tension transmitted by the tether is an important quantity, the assumption that the length between the two end-bodies follows Eq.2.57 implies that any variation in tether tension causing a deviation from Eq.2.57 is instantaneously corrected by the control system. Therefore, the kinematics of the tethered satellite under the planar dumbbell approximation are completely described by Eq.2.55 and Eq.2.57. Eq.2.55

gives the differential equation of motion in terms of both L and its derivatives and θ and its derivatives; Eq.2.57 prescribes L at any point in time. Substituting Eq.2.57 into Eq.2.55 gives

$$\ddot{\theta} - 2c(\dot{\theta} + \Omega) + \frac{3}{2}\Omega^2 \sin 2\theta = 0 \tag{2.59}$$

which is the tethered satellite equation of motion under an exponential reel-in control law. Misra and Modi showed that closed form solutions for the motion of a Planar Dumbbell tethered satellite exist if the equations of motion are linearized[5]. The angular motion of the tethered satellite must be small in order for the linearized equations of motion to approximate the nonlinear equations of motion. In order to generalize the following analysis, arbitrarily large angular displacements are considered, and therefore the linearized equations of motion and their closed form solutions are not considered to be accurate models of the tethered satellite physical behavior.

2.3.1 Nondimensionalizing the Equations of Motion

By the standard definition of angular measure in radians, the variable θ is nondimensional. Begin nondimensionalizing the other variables by defining the variable substitution

$$\tau = \Omega t \tag{2.60}$$

as suggested by Misra and Modi[5]. Taking the derivative of the angular variable θ with respect to τ yields

$$\frac{d\theta}{dt} = \frac{d\theta}{d\tau}\frac{d\tau}{dt} = \Omega\theta'$$

Hence

$$\dot{\theta} = \Omega\theta' \tag{2.61}$$

where $\dot{\theta} = \frac{d\theta}{dt}$ and $\theta' = \frac{d\theta}{d\tau}$ Similarly,

$$\ddot{\theta} = \Omega^2\theta'' \tag{2.62}$$

Also,

$$\frac{\dot{L}}{L} = -c = -\frac{c}{\Omega}\Omega = -\tilde{c}\Omega$$

where $\tilde{c}$ is a nondimensional variable equal to $\frac{c}{\Omega}$. Thus the non dimensional form of Eq.2.55 is

$$\Omega^2\theta'' - 2\tilde{c}\Omega(\Omega + \Omega\theta') + \frac{3}{2}\Omega^2 \sin 2\theta = 0$$

Simplification yields

$$\theta'' - 2\tilde{c}(1 + \theta') + \frac{3}{2}\sin 2\theta = 0 \tag{2.63}$$

2.3.2 Time Domain of the Equations of Motion

The equation of motion Eq.2.63 is valid over the entire time domain. However, it is important to note that the value of $\tilde{c}$ is not constant over the entire time domain. At

points in time at which the tether is not being reeled in, the value of $\dot{L}$, and thus the value of $\tilde{c}$, is zero and the tethered satellite equation of motion can be written as

$$\theta'' + \frac{3}{2}\sin 2\theta = 0 \tag{2.64}$$

which, under the variable substitution $\theta_s = 2\theta$ is

$$\theta_s'' + 3\sin\theta_s = 0 \tag{2.65}$$

which is the equation of a simple pendulum. This equation of motion is known to lead to either oscillatory or spinning behavior in physical space depending on the total energy of the system. This behavior is what is expected when the tethered satellite is not being reeled in. Therefore, if the reel-in process begins at $t > 0$, the phase plot of the system for points in time between $t = 0$ and the value of t for which the reel-in process begins is identical to that of a pendulum with the same set of initial conditions as those of the tethered satellite. Likewise, after the reel-in process is complete, the phase plot of the tethered satellite system for points in time after the reel-in process is complete is identical to that of a pendulum whose initial state is given by the state of the tethered satellite at the end of the reel-in period. In other words, the initial conditions for Eq.2.64 after the reel-in period is complete will be the angular displacement and speed of the tethered satellite at the point in time at which $\tilde{c}$ transitions from nonzero to zero.

2.3.3 State Space Equations of Motion and Definition of Nullclines

The analysis of the equation of motion will be carried out by determining the character of solution trajectories in the phase plane and then relating these trajectories to those in the $\theta - \tau$ plane. Begin by casting Eq. 2.63 into phase variable form and letting $x_1 = \theta$ and $x_2 = \frac{d\theta}{d\tau}$. This yields

$$x_1' = x_2 \tag{2.66}$$

$$x_2' = 2\tilde{c}(1 + x_2) - \frac{3}{2}\sin 2x_1 \tag{2.67}$$

The nullclines of a differential equation expressed in phase variable form are defined as the sets of points for which the time derivative of each state variable is exactly zero (therefore, an n^{th} order differential equation will have n nullclines). In the case of Eq.2.66 and Eq.2.67, the nullclines are the points satisfying

$$x_2 = 0 \tag{2.68}$$

or

$$x_2 = \frac{3}{4\tilde{c}}\sin 2x_1 - 1 \tag{2.69}$$

Using the standard terminology of differential equations, the sets of points defined by Eq.2.68 and Eq.2.69 will be referred to as the x_1-nullcline and x_2-nullcline, respectively[34]. Both equations have been solved for x_2 to facilitate their representation in

the phase plane ($x_1 - x_2$ space). In the phase plane, Eq.2.68 represents the abscissa (i.e. $x_2 = 0$) while Eq.2.69 represents a sinusoidal curve of amplitude $\frac{3}{4\tilde{c}}$ centered on the line $x_2 = -1$. The equilibria of Eq.2.55 occur where x_1' and x_2' are both zero; i.e., the equilibria occur at the intersections of the nullclines. By solving Eqs.2.68 and 2.69 simultaneously, it is found that the equilibria can only occur when

$$x_2 = 0 \tag{2.70}$$

and

$$x_1 = \frac{1}{2} \arcsin \frac{4\tilde{c}}{3} \tag{2.71}$$

The arcsin function is not defined if the argument is greater than 1 or less than -1; therefore, from Eq.2.70 and Eq.2.71 the system will have equilibria if and only if

$$x_2 = 0 \tag{2.72}$$

$$\text{and} \quad -\frac{3}{4} \leq \tilde{\text{c}} \leq \frac{3}{4} \tag{2.73}$$

Geometrically, the inequalities in Eq.2.73 give the range of $\tilde{c}$ values for which the sinusoidal x_2-nullcline intersects the x_1-nullcline. By inspection, if there is one intersection, then an infinite number of intersections exist from $x_1 = -\infty$ to $x_1 = \infty$. However, Eq.2.67 restricts the size of the interval of initial x_1 values for which the physical arrangement of the system is unique. For any angle ϕ, $\sin 2\phi = \sin 2(\phi + \pi)$. Therefore, because Eq.2.67 is dependent on $\sin 2x_1$, the maximum interval for which

this equation gives solutions that correspond to unique physical arrangements is of length π. In the interest of simplicity, the interval of initial x_1 values studied is $[-\frac{\pi}{2}, \frac{\pi}{2}]$.

Chapter 3

Analysis of the Nullclines and Equilibria

3.1 The Existence and Classification of Equilibria

From Eq.2.69 it can be seen that the graph of the x_2-nullcline sinusoid passes through the point (x_1, x_2) = (0, -1). In the case that the tether length is decreasing (i.e., $\dot{L} < 0$), it is known from Eq.2.63 that $\tilde{c}$ is positive; therefore, from Eq.2.69, the maximum value of the sinusoid occurs when $2x_1 = \frac{\pi}{2}$, i.e. when $x_1 = \frac{\pi}{4}$, and this maximum value is positive. Likewise, the next extrema of the sinusoid, which is a minimum, occurs at $2x_1 = \pi$, i.e. when $x_1 = \frac{\pi}{2}$, and this minimum is negative. Hence, from calculus, the Intermediate Value Theorem indicates that there is at least one point between (x_1, x_2) = (0, -1) and the subsequent maximum of the x_2-nullcline, at which the graph of the x_2-nullcline crosses the x_1-nullcline. Furthermore, the Intermediate Value Theorem also guarantees that there is at least one point between

this maximum and the subsequent minimum of the x_2-nullcline at which the graph of the x_2-nullcline intersects the x_1-nullcline. A sketch of Eq.2.69 indicates that both the transit from (x_1, x_2) = (0, -1) to the subsequent x_2-nullcline maximum and the transit from this maximum to the subsequent x_2-nullcline minimum each cross the x_1-nullcline exactly once. This indicates that there are two equilibria on the interval $[-\frac{\pi}{2}, \frac{\pi}{2}]$ if $\tilde{c} > \frac{3}{4}$. Because a maximum of two equilibria exist on the interval of interest and because they occur at two distinct points along the x_1 axis, they can be classified by their x_1 value. The equilibrium closer to the origin will be known as the lower equilibrium while the equilibrium with the equilibrium with the higher x_1 coordinate value will be known as the upper equilibrium. The equations of motion will be linearized about the equilibria in order to classify the equilibria.

A system of n linear differential equations can be expressed as

$$\vec{X}' = \mathbf{A}\vec{X} \tag{3.1}$$

where $\mathbf{A}$ is an $n \times n$ matrix, $\vec{X}$ is an $n \times 1$ vector and $\vec{X}'$ represents the vector derivative with respect to time. The linear system Eq.3.1 has a solution trajectory through phase space for each set of initial conditions X_o. The qualitative character of the solution trajectories can be determined by examining the eigenvalues of $\mathbf{A}$[34]. If $n = 2$, the system Eq.3.1 is known as a planar system and the character of the solution trajectories on the phase plane are well known[35].

The planar dumbbell model of a tethered satellite under an exponential reel-in law involves two state space differential equations making it a planar system. However, Eq.2.67 is nonlinear. Therefore, in order to classify the differential equations in the neighborhood of the equilibria, it is necessary to make a linear approximation of the state space equations of motions in the neighborhood of the equilibria. This is done using the variational equation

$$\vec{U}' = \mathbf{D}\vec{U} \tag{3.2}$$

where $\vec{U} = \vec{X}$ and $\mathbf{D}$ is the Jacobian of the equations of motion. The Jacobian of Eq.2.66 and Eq.2.67 is

$$\mathbf{D} = \begin{bmatrix} 0 & 1 \\ -3\cos 2x_1 & 2\tilde{c} \end{bmatrix} \tag{3.3}$$

The linearization of Eq.2.66 and Eq.2.67 is

$$\begin{bmatrix} x_1' \\ x_2' \end{bmatrix} = \begin{bmatrix} 0 & 1 \\ -3\cos 2x_1 & 2\tilde{c} \end{bmatrix} \begin{bmatrix} x_1 \\ x_2 \end{bmatrix} \tag{3.4}$$

If Eq.3.4 is evaluated at the x_1 values of the equilibria, the character of solutions in the neighborhood of each equilibrium can be determined. The eigenvalues of $\mathbf{D}$ are given by

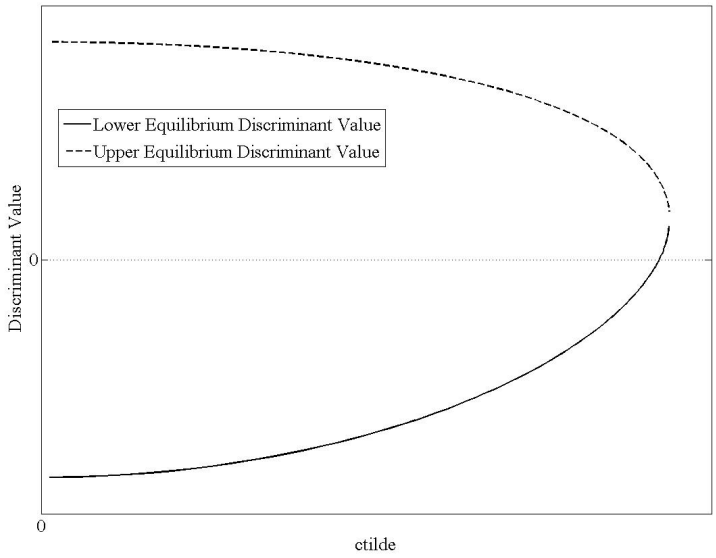

Figure 3.1: The value of the discriminant for the lower and upper equilibria versus $\tilde{c}$. Values below zero indicate the the eigenvalues will contain nonzero imaginary components. Values above zero indicate that the eigenvalues will be real.

$$\lambda_{1,2} = \tilde{c} \pm \sqrt{\tilde{c}^2 - 3\cos 2x_1} \tag{3.5}$$

Eq.3.5 can be used to calculate the value of the eigenvalues of the equations of motion evaluated at the equilibria resulting from any given value of $\tilde{c}$. Fig.3.1 shows the value of the discriminant of the characteristic equation of $\mathbf{D}$. By inspection of Eq.3.5, if this quantity is below zero, the eigenvalues of the system will have nonzero imaginary parts. Fig.3.1 shows that for most of the values of $\tilde{c}$ for which equilibria exist, the discriminant of the lower equilibrium (the equilibrium that is closest to the origin of the phase plane) is less than zero and thus the eigenvalues corresponding to

the lower equilibria have nonzero imaginary parts. Furthermore, Fig.3.1 shows that the discriminant of the eigenvalues corresponding to the upper equilibrium is greater than zero for all values of $\tilde{c}$ for which equilibria exist.

If the eigenvalues of the Jacobian matrix of a planar system evaluated at an equilibrium are determined to contain nonzero imaginary parts, the characteristic phase plane solution trajectories in the neighborhood of the equilibrium tend to spiral about the equilibrium[34]. Alternatively, if the eigenvalues are found to be real, the characteristic phase plane solution trajectories near the equilibrium tend to either proceed toward the equilibrium (this structure is known as a sink), away from the equilibrium (this structure known as a source), or toward the equilibrium along one state variable axis and away from the equilibrium along the other state variable axis (this structure is known as a saddle)[34]. The actual behavior depends on the sign of the real and imaginary parts of the eigenvalues. Fig.3.1 shows that for the equilibrium closest to the origin, the discriminant of Eq.3.5 is less than zero for almost all values of $\tilde{c}$ for which equilibria exist. Therefore, for any given value of $\tilde{c}$, solution trajectories in the neighborhood of the lower equilibrium will have a spiral structure around the equilibrium while solution trajectories in the neighborhood of the upper equilibrium will exhibit behavior characteristic of a saddle. Because of the characteristic structure around the equilibria, let the lower equilibrium also be known as the spiral

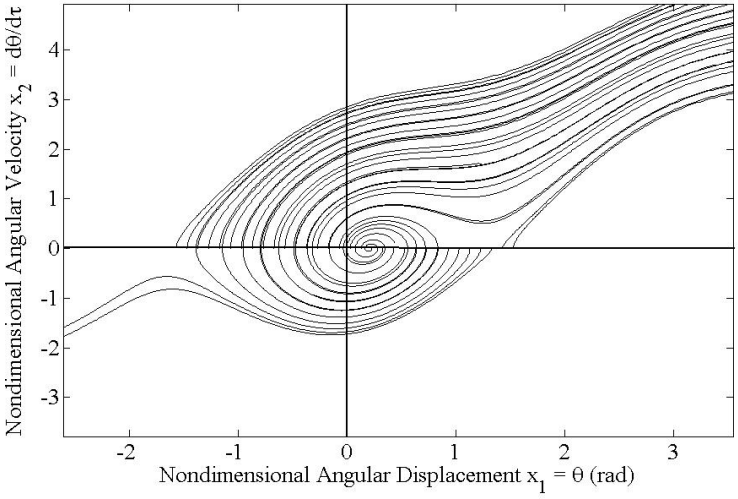

Figure 3.2: Solution trajectories in the phase plane

equilibrium and the upper equilibrium be known as the saddle equilibrium. The assertion concerning solution trajectory behavior in the neighborhood of an equilibrium is confirmed by numerically simulating solution trajectories in the phase plane. This simulation is shown in Fig.3.2.

3.2 General Solution Trajectory Behavior: Geometric Arguments

Each nullcline divides the phase plane into three sets: the set of points above the nullcline, the set of points below the nullcline, and the set of points making up the nullcline itself. Consider the second equation of motion Eq.2.67 and the corresponding

x_2-nullcline given by Eq.2.69. These three sets in the $x_1 - x_2$ plane are defined as the sets of points (x_1, x_2) satisfying

$$x_2 > \frac{3}{4\tilde{c}} \sin 2x_1 - 1 \tag{3.6}$$

$$x_2 < \frac{3}{4\tilde{c}} \sin 2x_1 - 1 \tag{3.7}$$

$$x_2 = \frac{3}{4\tilde{c}} \sin 2x_1 - 1 \tag{3.8}$$

where $x_1 \in (-\infty, \infty)$. These three sets will be referred to collectively as the x_2-nullcline-generated sets. The salient characteristic of these sets is the sign of x_2' at any point in each set. The sign of x_2' for points within each set can be determined by applying the appropriate inequality (Eq.3.6, 3.7, or 3.8) to Eq.2.67 and solving for x_2'. If the point (x_1, x_2) satisfies Eq.3.6, then x_2' is positive and x_2 increases as τ increases. If the point satisfies Eq.3.7, then x_2' is negative and x_2 decreases as τ increases. Finally, if the point satisfies Eq.3.8, then x_2' is exactly zero. This indicates that at that point, the tangent to the solution trajectory is parallel to the abscissa.

The same type of analysis can be applied to the x_1-nullcline given by Eq.2.68. The x_1-nullcline divides the plane into the sets

$$x_2 > 0 \tag{3.9}$$

$$x_2 < 0 \tag{3.10}$$

$$x_2 = 0 \tag{3.11}$$

These sets will be referred to as the x_1-nullcline-generated sets. If the point (x_1, x_2)

satisfies Eq.3.9, then, by Eq.2.66, x_1' is positive and x_1 increases with an increase in τ. If the point satisfies Eq.3.10, then x_1' is negative and x_1 decreases with an increase in τ. If the point satisfies Eq.3.11, then x_1' is zero and the local tangents to the solution trajectories are vertical.

3.3 General Solution Trajectory Behavior: Derivative Arguments

Alternatively, the derivative of x_2 with respect to x_1 can help determine the shape of the solution trajectories. This will yield local slopes of trajectories in the $x_1 - x_2$ plane. The solution trajectories that are plotted in the phase plane each correspond to a different initial condition and each solution trajectory is known as a *flow* in the standard terminology of nonlinear dynamics[34]. The flow of a set of differential equations in the phase plane is denoted by $\phi_t(X_o)$ where X_o is a vector expression of the initial state of the system. The derivative arguments made below are valid for each flow in the phase plane, i.e., solution trajectories corresponding to each set of initial conditions. In order to calculate this derivative, cast it in the form

$$\frac{\partial x_2}{\partial x_1} = \frac{\frac{\partial x_2}{\partial \tau}}{\frac{\partial x_1}{\partial \tau}} = \frac{x_2'}{x_2} \tag{3.12}$$

from which

$$\frac{\partial x_2}{\partial x_1} = 2\tilde{c}(1 + \frac{1}{x_2}) - \frac{3}{2x_2}\sin 2x_1 \tag{3.13}$$

is obtained. From Eq.3.13 it can be seen that as the angular velocity x_2 approaches zero, the derivative $\frac{\partial x_2}{\partial x_1}$ increases without bound provided x_2' does not approach zero, as would be the case near to an equilibrium point. Therefore, an angular velocity x_2 approaching zero indicates that the solution trajectories are locally parallel to the x_2 axis. Furthermore, from Eq.3.13, the necessary and sufficient conditions for positive, negative, and zero $\frac{\partial x_2}{\partial x_1}$ are as follows:

$$\frac{\partial x_2}{\partial x_1} > 0 \Leftrightarrow x_2 > \frac{3}{4\tilde{c}} \sin 2x_1 - 1 \tag{3.14}$$

$$\frac{\partial x_2}{\partial x_1} < 0 \Leftrightarrow x_2 < \frac{3}{4\tilde{c}} \sin 2x_1 - 1 \tag{3.15}$$

$$\frac{\partial x_2}{\partial x_1} = 0 \Leftrightarrow x_2 = \frac{3}{4\tilde{c}} \sin 2x_1 - 1 \tag{3.16}$$

These conditions are identical to Eqs.3.6 - 3.8 and hence the sets generated by Eqs.3.14 - 3.16 represent the same sets expressed by Eqs.3.6 - 3.8, i.e. the nullcline-generated sets.

The x_1-nullcline is identical to the x_1 axis. This nullcline simply indicates the boundary at which x_1' changes sign. Because x_1' is defined to be x_2, the sign of a change in x_1 with respect to τ is the same as the sign of x_2. Therefore, since x_2 is positive in the upper half plane, the trajectories increase in x_1 as τ increases, i.e. they tend toward the right in the phase plane. Similarly, in the lower half plane, where x_2 is negative, the trajectories decrease in x_1 as τ increases, i.e. they tend toward the left in the phase plane. On the x_1-nullcline, the tangents of the solution trajectories

are locally vertical as discussed earlier in this section.

3.4 Classification of Regions of the Phase Plane

As stated above using both geometric and derivative arguments, the x_1 and x_2-nullclines each divide the phase plane into three sets (the nullcline-generated sets). Given a point (x_1, x_2), the local tendency of the x_1 component of the solution trajectory containing that point is given by the location of the point relative to the x_1-nullcline. Likewise, the local tendency of the x_2 component is given by the location of the point relative to the x_2-nullcline. Therefore, the behavior of a tethered satellite system with respect to θ and $\dot{\theta}$ can be determined at any point in time by examining the corresponding values of x_1 and x_2 at that time and determining the nullcline-generated set to which the point (x_1, x_2) belongs.

The intersection of the first x_2-nullcline-generated set with the first x_1-nullcline-generated set represents the set of points (x_1, x_2) that are located above both the x_1-nullcline and the x_2-nullcline. According to previous arguments, solution trajectories passing through these points will locally proceed to the left (in the direction of increasing x_1) and upwards (in the direction of increasing x_2) in the phase plane. This region is labeled Region 1 on Fig.3.3. In this region the tethered satellite moves counterclockwise with respect to the orbital axes and its angular speed is increasing.

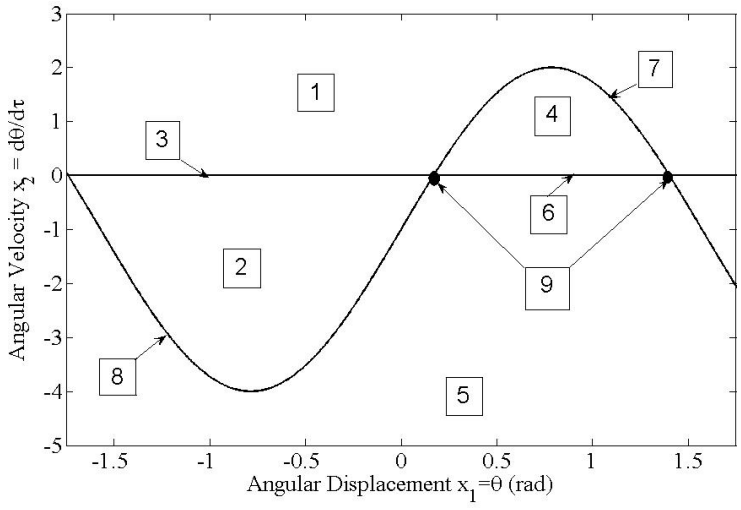

Figure 3.3: The regions of the phase plane determined by the x_1 and x_2-nullclines

The intersection of the first x_2-nullcline-generated set with the second x_1-nullcline-generated set is labeled as Region 2 on Fig.3.3 and represents solution trajectories that are increasing in x_2 but decreasing in x_1. This represents an overall solution trajectory motion toward the upper right in the phase plane. If the point (x_1, x_2) is in this region the tethered satellite moves clockwise with an increasing angular speed. The intersection between the first x_2-nullcline-generated set and the third x_1-nullcline-generated set is labeled Region 3 on Fig.3.3; at these points, the tangent of the solution trajectories is vertical and the trajectories are increasing in x_2. If the tethered satellite is in this state, the angular speed of the tethered system is instantaneously zero but increases after a short amount of time. These points indicate a change in the direction of θ from a negative (clockwise) direction to a positive

(counterclockwise) direction.

The intersection of the second x_2-nullcline-generated set with the first x_1 set is labeled Region 4 on Fig.3.3 and represents points that are above the x_1-nullcline but below the x_2-nullcline. As such, solution trajectories passing through these points locally proceed downward and rightward in the phase plane. Physically, this indicates a tethered satellite system moving counterclockwise, but decreasing in angular speed. The intersection of the second x_2-nullcline-generated set with the second x_1-nullcline-generated set represents points that are below both nullclines. These points proceed downward and to the left in the phase plane. The set of points at which this occurs are labeled Region 5 on Fig.3.3. A tethered satellite operating in this region of the phase plane moves clockwise with increasing angular speed. The intersection of the second x_2-nullcline-generated set with the third x_1-nullcline-generated set describes points that are on the x_1-nullcline and below the x_2-nullcline. The tangent of the solution trajectories passing through these points is vertical and the trajectories themselves decrease in x_2. This results in a downward motion in the phase plane; points at which this occur are labeled Region 6 on Fig.3.3. A tethered satellite operating in Region 6 has an instantaneously zero angular speed that decreases after a small amount of time. Physically, this corresponds to a direction change from counterclockwise motion to clockwise motion.

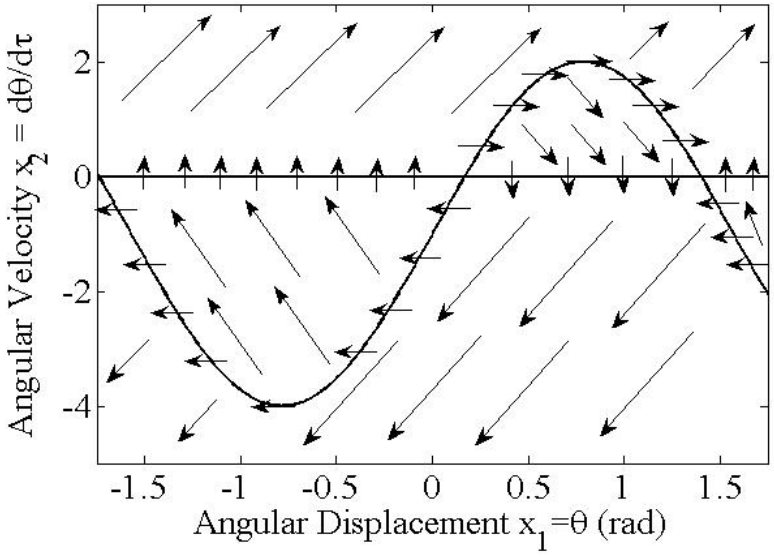

Figure 3.4: The tendencies of the solution trajectories in each region of the phase plane. In each of the regions of the phase plane, the solution trajectories tend to progress in the direction indicated by the arrows.

The final intersections to consider are the intersections of the third x_2-nullcline-generated set with the x_1-nullcline-generated sets. These intersections all lie along the x_2-nullcline and thus proceed horizontally in the phase plane. Trajectories passing through points in the intersection of the third x_2-nullcline-generated set and the first x_1-nullcline-generated set are located above the x_1-nullcline. Therefore, these trajectories proceed purely in the direction of increasing x_1, or rightward in the phase plane. These points are labeled Region 7 on Fig.3.3. The states comprising Region 7 correspond to a tethered system with angular acceleration of zero and positive angular velocity indicating counterclockwise movement. Similarly, points lying in the intersection of the third x_2-nullcline-generated set and the second x_1-nullcline-generated set are located below the x_1-nullcline and proceed in the direction of decreasing x_1, or leftward in the phase plane without moving vertically, i.e., locally these trajectories are horizontal in the phase plane. This is Region 8 on Fig.3.3. Again, the tethered satellite angular acceleration in Region 8 is zero, but the angular displacement is clockwise. Finally, the intersection between the third x_2-nullcline-generated set and the third x_1-nullcline-generated set represents points that lie on both nullclines. These points are equilibrium points and are labeled as Region 9 on Fig.3.3. Tethered systems operating in this regime experience tether length contraction, but do not experience angular displacement. Each of these tendencies is shown on Fig.3.4. Information regarding each of the regions and the tendencies of solution trajectories

Region	Relationship to:		Phase Plane Direction	Region Type
	x_1-nullcline	x_2-nullcline		
1	Above	Above	Upper Right	Space
2	Below	Above	Upper Left	Space
3	On	Above	Up	Line
4	Above	Below	Lower Right	Space
5	Below	Below	Lower Left	Space
6	On	Below	Down	Line
7	Above	On	Left	Line
8	Below	On	Right	Line
9	On	On	No Movement	Disjoint Points

Table 3.1: Region Definitions and Solution Trajectory Tendencies Therein

passing through those regions is summarized in the table below.

Chapter 4

Global Solution Trajectory Behavior

4.1 Trajectory Behavior Near Nullclines: Spiraling Behavior

If the value of $\tilde{c}$ satisfies the condition

$$-\frac{3}{4} < \tilde{c} < \frac{3}{4} \tag{4.1}$$

then, from Eq.2.69 it can be seen that the maxima of the x_2-nullcline will be located above the x_1-nullcline, since the x_2-nullcline is centered on $x_2 = -1$. This implies that the set of points described by Regions 4 and 6 in Fig.3.3 will not be empty. Furthermore, since the set of $\tilde{c}$ values determined by Eq.4.1 is a subset of the set determined by Eq.2.73, equilibria will exist if Eq.4.1 is satisfied. The number and type of equilibria along the interval of interest has previously been discussed in Section 3.1.

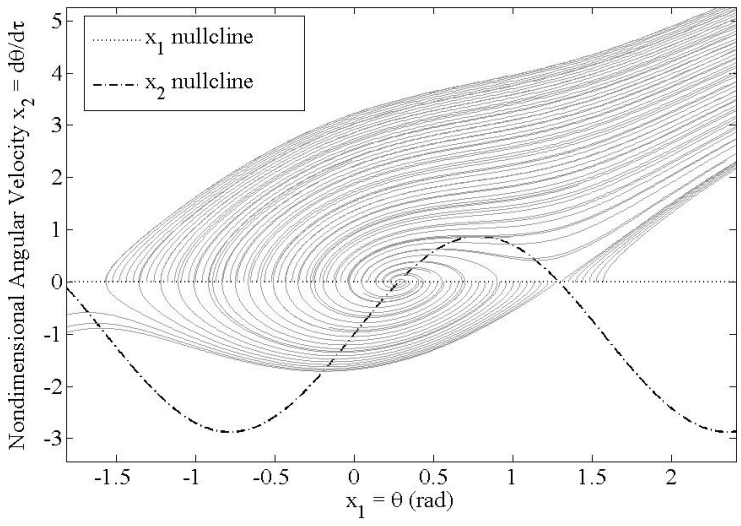

Figure 4.1: Spiraling behavior near the spiral equilibrium for the case $\tilde{c} < \frac{3}{4}$

Consider a solution trajectory whose initial conditions are located in Region 6 near the leftmost equilibrium. If x_2 at $\tau = 0$ is zero, then the local tangents to the solution trajectories are initially vertical. As the trajectories proceed, they move out of Region 6, i.e., off of the x_1-nullcline and into Region 5, where they proceed downward and to the left. Some of these trajectories intersect the x_2-nullcline during this transit and move from Region 5 to Region 8, where the tangent to the solution trajectory is horizontal. After the intersection with the x_2-nullcline, the trajectories move into Region 2 where they proceed upward and to the left. These trajectories then intersect the x_1-nullcline (Region 3), where they are locally vertical, and then move into Region 1 where they proceed upward and to the right. Some of these trajectories may move from Region 1 across the x_2-nullcline into Region 3; this pattern of motion

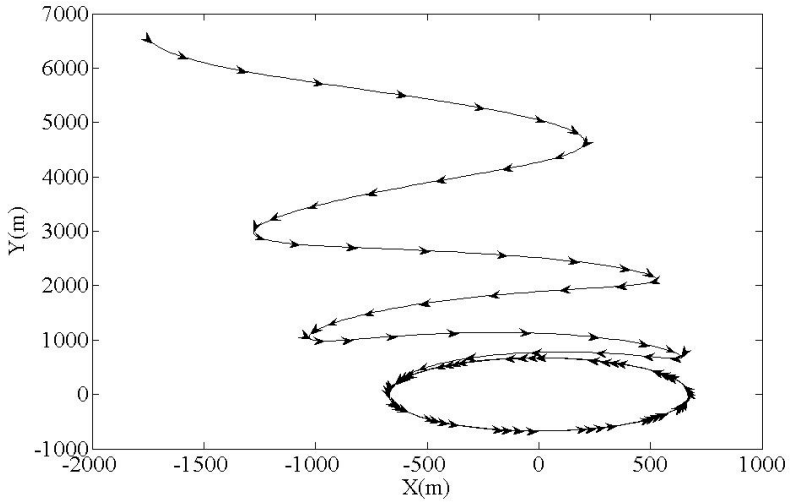

Figure 4.2: The path of an end-body whose solution trajectory circulates around the spiral equilibrium plotted with respect to the orbital axes. Note that the arrows show the direction of the velocity and are spaced at equal time intervals.

describes a clockwise movement of trajectories about the equilibrium. This spiral structure is a prominent feature of numerical simulations and is shown in Fig. 4.1. The fact that solution trajectories spiral around the equilibrium implies an oscillation in the value of x_2. Such an oscillation indicates that, in physical space, the angular displacement of the satellite from the local vertical does not increase quickly. The equilibrium around which solution trajectories tend to spiral will be known as the *spiral equilibrium.*

The spiraling solution trajectory described above implies an oscillation of the tethered satellite system about the spiral equilibrium point. Fig.4.2 shows the path through space of the end body that starts farthest away from the Earth. For this

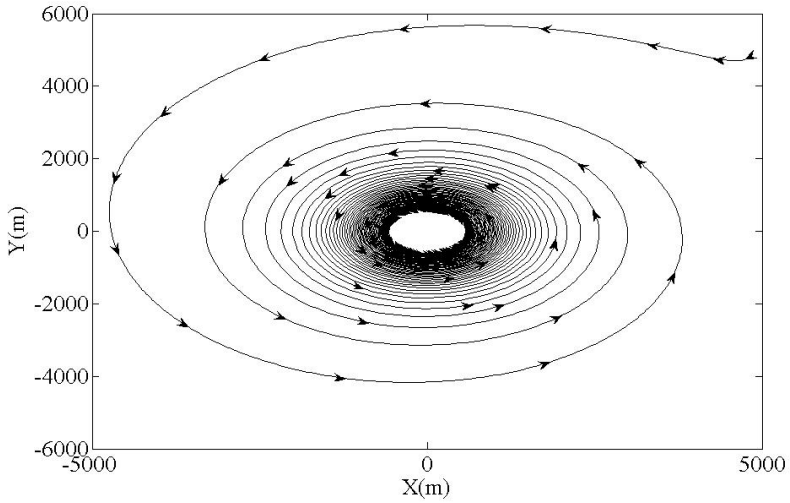

Figure 4.3: The path of an end-body whose solution trajectory does not circulate around the spiral equilibrium plotted with respect to the orbital axes. As in Fig.4.2, the arrows show the direction of the velocity and are spaced at equal time intervals.

simulation, the initial angular displacement is 20 degrees and the x_1 value at which the spiral equilibrium occurs is, to two decimal places, 31.01 degrees. Note the points at which the tangent to the trajectory is vertical. These points represent zeros in angular velocity and occur as the tethered satellite system changes direction. Compared to Fig.4.3, which shows the path through space of the end body of a tethered satellite whose solution trajectory does not circulate around the spiral equilibrium, the motion shown in Fig.4.2 is more erratic. Fig.4.4 shows the angular velocity of the tethered satellite system with the circulating solution trajectory as a function of time. This graph is much less smooth than Fig.4.5, which shows the angular velocity of the non-circulating solution trajectory case as a function of time. Each of these graphs

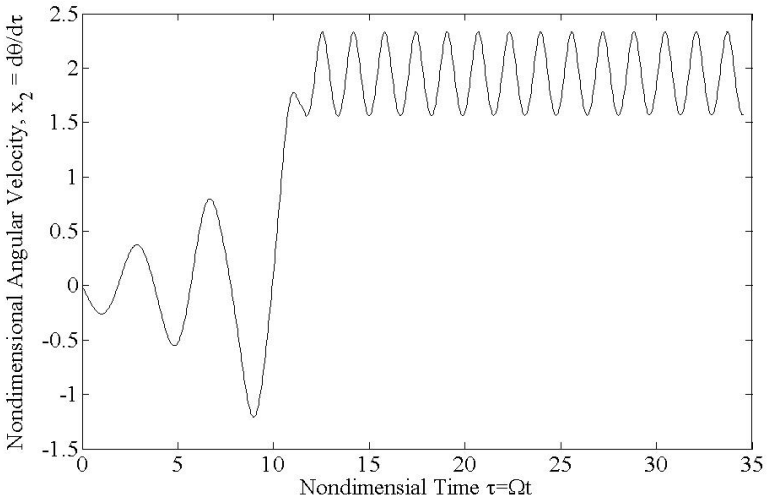

Figure 4.4: Angular velocity of an end-body whose solution trajectory circulates around the spiral equilibrium. Note the periodic nature of the velocity at larger values of τ.

contains a transitional point at which the tether stops reeling in and the steady state motion of the tethered satellite system is reached.

The existence of an equilibrium around which solution trajectories circulate raises the possibility of the existence of a space in the phase plane in the vicinity of the spiral equilibrium inside which no solution trajectory travels far enough away from the equilibrium to indicate that the tethered satellite angular displacement increases as a function of time. Indeed, this region exists and examples of these trajectories are shown in Fig.4.6. Solution trajectories in this region correspond to states which do not deviate appreciably from their initial conditions while the tethered satellite is being reeled in. In this region, it can be seen that after the reel-in process is complete,

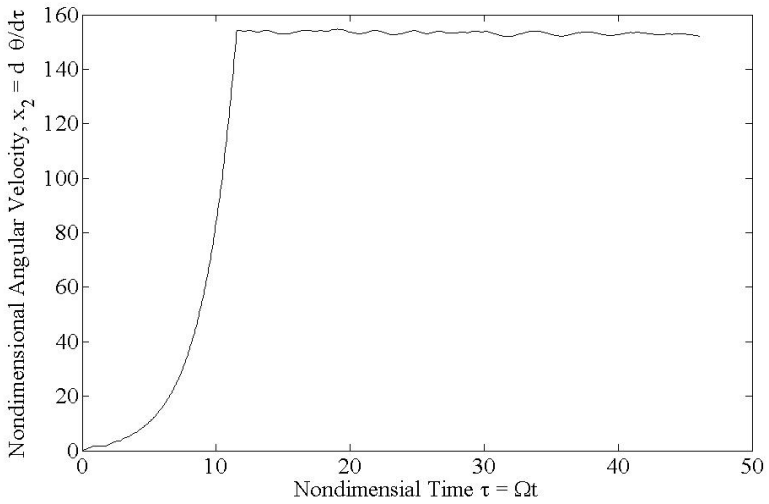

Figure 4.5: Angular velocity of an end body whose solution trajectory does not circulate around the spiral equilibrium. Note the stable behavior compared to Fig.4.4.

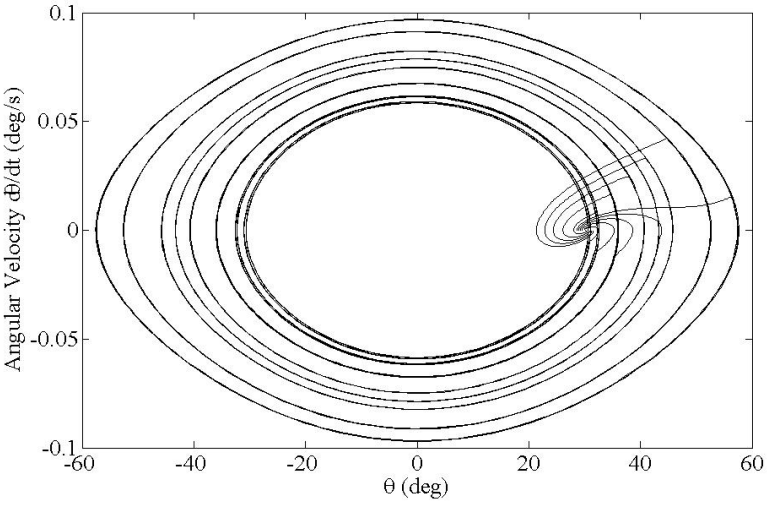

Figure 4.6: Solution trajectories of a tethered satellite system that does not enter a spin when the reel-in program is complete.

the tethered system does not have enough angular momentum to overcome the effect of the gravitational gradient, and simply oscillates about the spiral equilibrium in a pendular motion. Since this behavior is not desirable, mission planners should avoid trajectories that originate, or otherwise pass near the spiral equilibrium. Numerical simulations of proposed solution trajectories can be used to determine the closest passage of a proposed trajectory to the spiral equilibrium; using this information, the mission planner can determine whether or not the solution trajectory is appropriate for a given mission.

4.2 Trajectory Behavior Near Nullclines: Constant Direction Behavior

There are many solution trajectories that pass near nullclines but do not intersect them. The properties of these trajectories at points on the phase plane, however, are still related to the relationship between the solution trajectory and the nullclines. Upon inspection of Fig. 4.7, a relationship between the location of the maxima and minima of the x_2-nullcline can be seen. According to Eq.3.13, the solution regime in which x_2 is small (i.e. where the solution trajectory is close to the abscissa, and thus is close to the nullclines) is dominated by the terms $\frac{2\tilde{c}}{x_2}$ and $-\frac{3}{2x_2}\sin 2x_1$. The oscillatory term $-\frac{3}{2x_2}\sin 2x_1$ can be compared to the oscillatory term $\frac{3}{4\tilde{c}}\sin 2x_1$ in Eq.2.69. These

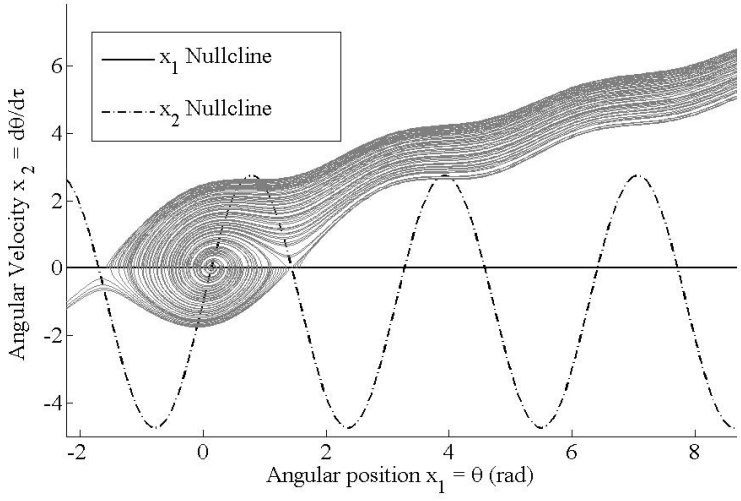

Figure 4.7: The behavior of solution trajectories near the nullclines. Note the relationship between the solution trajectory and the value of the x_2-nullcline at each value of x_1.

terms oscillate in x_1, but are completely out of phase with each other due to the fact that one has a negative coefficient while the other has a positive coefficient. As a result, for constant values of x_2, the value of $\frac{\partial x_2}{\partial x_1}$ is a maximum at minimum values of the x_2-nullcline and the value of $\frac{\partial x_2}{\partial x_1}$ is a minimum at maximum values of the x_2-nullcline. This is illustrated by Fig.4.7 and can be used as a qualitative rule to determine the approximate behavior of solution trajectories in Regions 1 and 5 that do not intersect either nullcline.

4.3 Trajectory Behavior Far From Nullclines

Far from the nullclines (i.e. at large positive or negative values of x_2), Eq.3.13 indicates that the dominant term in the slope of the trajectories is the constant term $2\tilde{c}$. This suggests that for large angular velocities, a differential equation approximating the tethered satellite angular motion can be written as follows

$$\frac{dx_1}{d\tau} = 2\tilde{c}x_1 \tag{4.2}$$

The solutions to this equation are given by

$$x_1(\tau) = x_1(\tau_c)e^{2\tilde{c}(\tau-\tau_c)} \tag{4.3}$$

where τ_c is the point in time at which the approximation is to begin; in order to approximate the solution trajectory well, this would be a value of time after which the solution trajectory is far from either nullcline. This solution indicates an exponential rise in x_1 as τ increases. Therefore, while the tethered reel system is reeling the tether in, the angular displacement (and thus angular velocity and acceleration) can be approximated by an exponential function. Fig.4.8 shows this approximation in the phase plane while Fig.4.9 shows this approximation in $x_1 - \tau$ space.

The exponential relationship expressed in Eq.4.3 can be used to estimate the value of $\frac{L_i}{L_f}$ required to reach a desired value of x_2 for a tethered satellite with a given nondimensional tether reel-in time $\tau_r = t_r\Omega$. Such an estimation tool can be valuable to mission planners as will be demonstrated using case studies. In order to make this

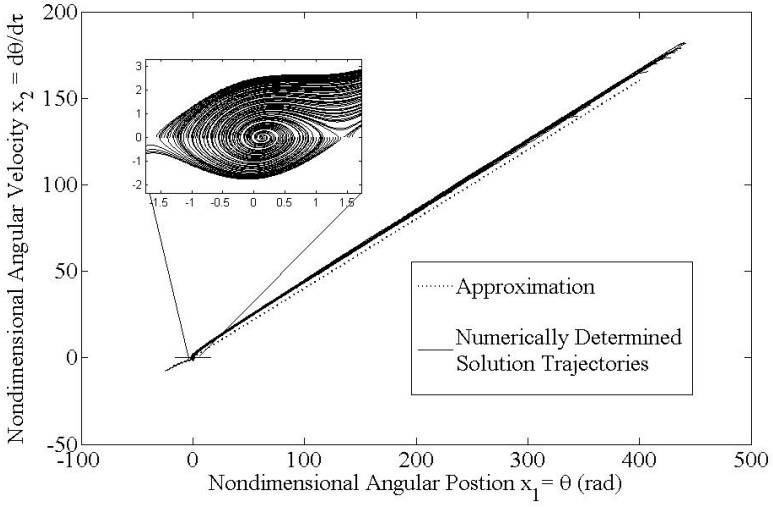

Figure 4.8: The behavior of solution trajectories far from the nullclines plotted with the approximation described by Eq.4.3.

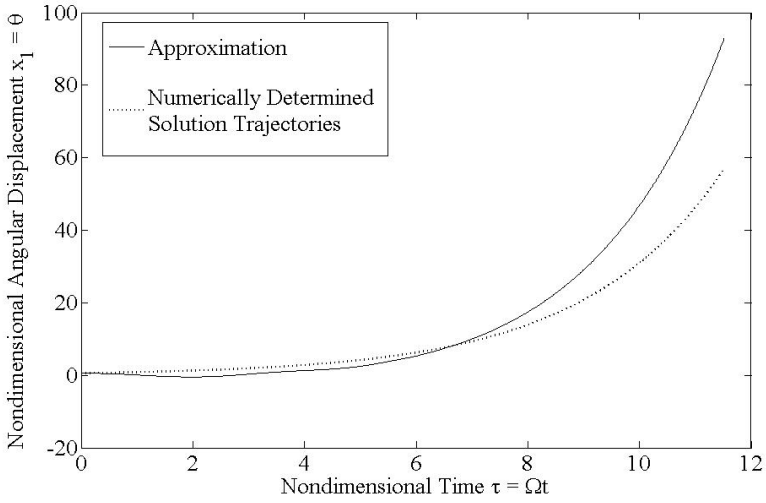

Figure 4.9: A sample solution far from the nullclines in the $x_1 - \tau$ plane plotted with the approximation described by Eq.4.3. Note that τ_c in Eq.4.3 is zero.

estimation, first differentiate Eq.4.3 with respect to time. This differentiation yields

$$x_2(\tau) = 2x_1(\tau_c)\tilde{c}e^{2\tilde{c}\tau-\tau_c} \tag{4.4}$$

In order to determine the value of x_2 at the end of the tether reel-in period, let $\tau - \tau_c = \tau_r$. Combining the definition of $\tilde{c}$, Eq.2.63, with Eq.4.4 yields

$$x_2(\tau_r) = 2\frac{ln\frac{L_i}{L_f}}{\tau_f}x_1(0)(\frac{L_i}{L_f})^2 \tag{4.5}$$

In the case of a tethered satellite with a contracting tether, the ratio $\frac{L_i}{L_f}$ is larger than unity; therefore, the square of the ratio changes more quickly than the natural logarithm of the same ratio. From Eq.4.5 it can be seen that the angular velocity of the tethered satellite approximately scales with the square of the ratio of the initial tether length to the final tether length. Using this relationship as a general guideline, the approximation

$$\frac{L_i}{L_f} \approx \sqrt{x_2} \tag{4.6}$$

can be used to estimate the ratio $\frac{L_i}{L_f}$ required to reach a certain value of x_2 insofar as the basic assumptions of the initial approximation Eq.4.3 are valid, i.e., assuming that the state of the system at the beginning of the approximation is not near the nullclines on the phase plane.

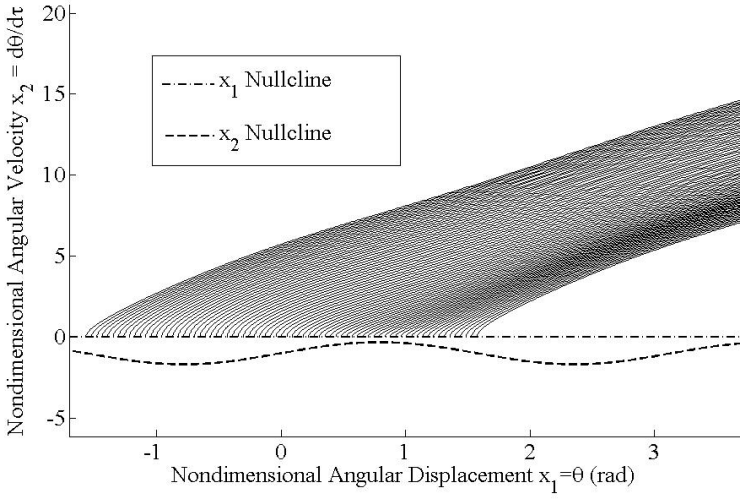

Figure 4.10: Solution trajectories in the case $\tilde{c} > \frac{3}{4}$. Note the uniform behavior of the trajectories.

4.4 Trajectory Behavior in the Regime $\tilde{c} > \frac{3}{4}$

If $\tilde{c} > \frac{3}{4}$, then Eq.2.71 has no solutions, indicating that there are no equilibria on the interval $[-\frac{\pi}{2}, \frac{\pi}{2}]$. Eq.2.69 indicates that if $\tilde{c} > \frac{3}{4}$ the amplitude of the sinusoidal nullcline is less than 1. This indicates that the maximum x_2 value that the nullcline can possibly reach is less than zero since the sinusoid is centered on $x_2 = -1$. Therefore, all solution trajectories are initially above the x_2-nullcline since $x_2(0) = 0$; hence the solution trajectories all initially lie in Region 3. The tangent of solution trajectories in this region (which constitutes a line in the phase plane) are locally vertical and the trajectories themselves proceed upward. Therefore, the trajectories move from Region 3 into Region 1. In Region 1, solution trajectories proceed upward and to

the left in the phase plane. Trajectories exhibiting this motion will not intersect any other nullcline at any point in time. Therefore, these solution trajectories continue to increase in the x_1 direction and the x_2 direction without bound, i.e. all solution trajectories correspond to a tethered satellite system spinning-up in the positive θ direction with no changes in angular direction or in the sign of angular speed. This behavior is shown in Fig.4.10.

This regime has great significance for the tethered system. If $\tilde{c} > \frac{3}{4}$, the operating regime of the system will exist solely in Regions 1 and 3 for all time, provided that the initial angular velocity is zero. This guarantees that the angular acceleration will monotonically increase while the tether length is decreasing. This provides for a smoother variation in angular velocity than would occur if the system solution trajectory circulated about a spiral equilibrium. Furthermore, the restriction that $\tilde{c} > \frac{3}{4}$ eliminates both equilibria, thus if $\tilde{c}$ is greater than $\frac{3}{4}$, the system will spin up to some nonzero average angular velocity regardless of its initial angular displacement away from the local vertical.

4.5 Considerations for $x_2(\tau = 0) \neq 0$

For the preceding discussions, the value of x_2 at $\tau = 0$, and thus $\dot{\theta}$ at $t = 0$ was assumed to be zero. However, the analysis of the tendencies of the solution trajectories in the various regions of the phase plane does not depend on this assumption.

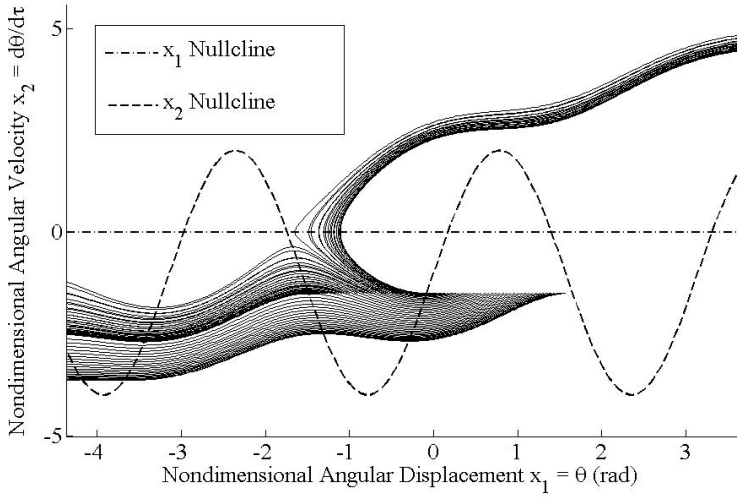

Figure 4.11: Phase plot where the initial angular velocity is less than zero. The trajectories behave according to the same rules described in Table 3.1 regardless of the initial velocity of the system.

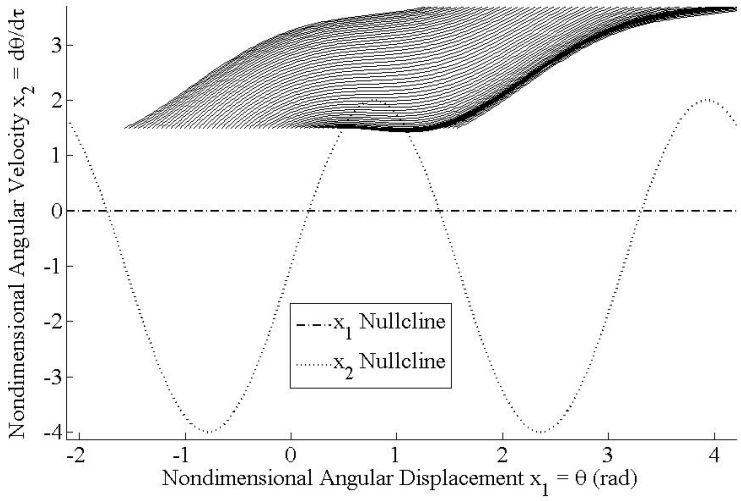

Figure 4.12: Phase plot where the initial angular velocity is greater than zero. Again, the trajectories behave according to the same rules described in table 3.1 regardless of the initial velocity of the system.

Therefore, each of the arguments above is general with respect to the initial value of x_2. Figs.4.11 and 4.12 show solution trajectories assuming that x_2 is greater than zero and less than zero, respectively. The dynamics in each situation are very different, but the solution trajectories obey the rules previously set forth.

Chapter 5

Applied Nullcline Analysis and Case Studies

5.1 Applications of Nullcline Analysis

Nullcline analysis, as it applies to tethered satellites contracting under an exponential control law, can be used by mission designers as a tool to evaluate possible initial conditions and physical parameters of a tethered satellite mission. The effects of changes in physical parameters for such tethered satellites under the planar dumbbell approximation are manifested through changes in the nondimensional parameter $\tilde{c}$. According to Eq.2.69, changes in $\tilde{c}$ result in changes to the amplitude of the x_2-nullcline. In fact, as $\tilde{c}$ increases from 0 to $\frac{3}{4}$, there is a bifurcation in the equations of motion. At a $\tilde{c}$ value of $\frac{3}{4}$, a single equilibrium appears at $(x_1, x_2) = (\frac{\pi}{4}, 0)$. At $\tilde{c}$

values greater than $\frac{3}{4}$, two equilibria exist. Assuming that a tethered satellite system mission design requires a tethered satellite reel-in without angular (spinning) motion, the presence of equilibria is essential and the mission parameters (L_o, L_i, Ω, t_r) should be selected such that $\tilde{c}$ is less than $\frac{3}{4}$. Alternatively, if a mission calls for a monotonic increase in the angular velocity of the system, the mission parameters should be chosen such that $\tilde{c}$ is greater than $\frac{3}{4}$. This will guarantee that no equilibria exist and that all solution trajectories increase in θ at an approximately exponential rate (See Sections 4.3 and 4.4).

Beyond simple mission design, nullcline analysis can be used to determine the effects of unforeseen errors that occur within a mission. For example, assume that a mission requires equilibria to ensure that a tethered satellite does not exhibit an angular displacement beyond a certain tolerance during the reel-in program. Further assume that while in orbit there is a change in $\tilde{c}$ from the value for which the system was designed. Such a change in $\tilde{c}$ can be the result many different types of malfunctions. Increased tether tension in the reel-in mechanism can result in a longer tether reel-in time t_r which raises the value of $\tilde{c}$. A jam in the tether reel-in system can result in a shorter final tether length L_f than was expected for the mission; such a malfunction lowers the value of $\tilde{c}$. An orbital insertion into a lower or higher orbit than was expected in the mission design also has the effect of lowering or raising $\tilde{c}$ respectively. If engineers can detect an error in the physical characteristics of the

tethered satellite system, the resulting nullclines can be plotted on phase space and the new equilibria can be calculated using Eq.2.71. The initial conditions for the new tethered satellite configuration can then be altered so that the mission may continue with a minimum change in dynamic behavior. In the case that the initial conditions cannot be changed, a decision can be made as to whether to abort the mission or proceed with the new mission dynamics.

5.2 Case Studies: The Tethered Artificial Gravity Satellite

5.2.1 Introduction to Artificial Gravity and the Tethered Artificial Gravity System

One proposed application of tethered satellites is to create a sense of artificial gravity in Earth orbit. There are several reasons for wanting to create artificial gravity in the microgravity environment. Astronaut health and comfort is greatly affected by the presence and level of a perceived gravitational field. Astronauts in orbit for long periods of time experience bone loss, muscle atrophy, and other side effects because of the lack of a perceived gravitational field in space. In fact, there is a reconditioning period that astronauts must undergo when they return to Earth from

a prolonged stay in orbit. The shortening or elimination of this reconditioning period would be beneficial to Mars mission planners as a reconditioning period upon an astronaut's arrival to Mars may not be practical. Furthermore, there is an interest in observing the response of biological processes to lower (but nonzero) gravitational effects. Therefore, the presence of a variable gravity laboratory would be of interest to the space program. Such systems have been studied by many researchers in the past[36, 37, 38, 39, 40]. Another such system is the Tethered Artificial Gravity system proposed by Hoffman and Mazzoleni[36].

The Tethered Artificial Gravity (TAG) concept involves two end bodies attached by a tether. The purpose of the TAG system is to produce an artificial gravitational force on masses located within the satellite end-bodies. This is accomplished by taking advantage of the centripetal acceleration required to keep a mass moving along a circular path. The TAG system is designed to cause the satellite end bodies to rotate about a common center of mass, i.e. to cause each of the end-bodies to move along a circular path. In order to achieve circular motion, a tension force is exerted on each end-body along the tether toward the center of mass. This force induces the centripetal acceleration necessary to move the end-body along a circular path. Because free masses within the end-body will tend to move in a straight line with respect to an inertial reference frame unless acted upon by a force (Newton's First Law), a force must be applied to these masses to cause them to move in a circular

path. This centripetal acceleration is imparted to the free masses by the end-body itself through a normal force. This normal force is analogous to the normal force that would be imparted by a fixed surface in response to a weight applied perpendicular to that surface. Therefore, when free masses within the end-body are accelerated in a circular path, the normal (centripetal) force applied to the free masses is identical to the normal force that would be imparted to the free mass by a fixed surface provided that a weight of magnitude

$$W = m\omega^2 r \tag{5.1}$$

were acting on the fixed surface. In Eq.5.1, m is the mass of the free mass, ω is the rotational rate of the system, and r is the distance between the free mass and the center of rotation. In this manner, the TAG system is capable of applying an artificial gravitational force to free masses located within the end-bodies.

The planar dumbbell tethered satellite model captures the essential dynamics of the TAG system, and therefore, the following case studies will make use of this model to describe TAG system dynamics. The two TAG end-bodies are modeled as point masses and they are connected by a massless, inextensible tether. The only forces considered to act on the TAG system are the gravitational force between each end mass and the Earth and the tension forces that travel through the tether. The satellite motion is assumed to take place entirely in the orbital plane. This two dimensional model uses the coordinates L to describe the distance of points from the center of

mass and θ to describe the angular displacement of the tether axis away from the local vertical. The tether length control law that will be assumed for the analysis is an exponential control law.

5.2.2 Case Study 1: Lunar Gravity Simulation

Consider a TAG system designed to impart an artificial gravitational force of $\frac{1}{6}g$ (the gravitational acceleration on the surface of the Moon) to masses located inside the end-bodies. Such a system would provide a laboratory in which to study the effect of reduced lunar gravity on mechanical, thermal, and biological systems and would provide a precursor to a manned lunar base. The artificial gravity imparted to masses in the end-bodies is related to the rotational speed of the masses about the center of mass of the tethered satellite system. Assume that the TAG system is designed to impart this artificial gravitational force to humans. It is known that the maximum rotational rate that humans can withstand without disorientation due to Coriolis forces is approximately 1 rotation per minute (rpm)[41]. Therefore, assume that the desired angular velocity of the TAG system is 1 rpm, or 0.1047 rad/s. The magnitude of the acceleration toward the center of mass, and hence the artificial gravitational acceleration imparted to masses in the end-bodies, is

$$a_c = \omega^2 r \tag{5.2}$$

where ω is the angular speed of the TAG system and r is the distance between the TAG center of mass and the end-body. Assume that the end-bodies are equal in mass, so that the center of mass of the TAG system is located in the geometric center of the tether. From Eq.5.2, it can be seen that, under an angular velocity of 0.1047 m/s^2, the TAG final tether length (system diameter) necessary to achieve an acceleration of $\frac{1}{6}g$ is 298 meters; let this be the target final tether length.

The next parameter that can be determined is the tether reel-in time. Assume a priori that the tether reel-in process takes 30 minutes. Also assume that, as before, the tether is orbiting at an orbital radius of 6878 kilometers from the center of the Earth. Finally, assume that for the TAG system, it is desirable for every solution trajectory to enter some level of spin-up, no matter what the initial displacement from the local vertical is. Assuming that initially the TAG system has a positive or zero angular velocity, this implies that $\tilde{c}$ must be greater than $\frac{3}{4}$. From Eq.2.71, it is known that the minimum value of L_i that can be used to meet the restriction on $\tilde{c}$ is 1316 meters; however, numerical simulation of the TAG system under these conditions reveals that if the initial tether length is set at 2991 meters, the final target angular speed value of 0.1047 radians per second will not be met. Eq.4.6 suggests that the choice of an initial tether length of 10 times the final tether length will result in a final angular speed value greater than 0.1047 radians per second. Numerical simulations confirm this assessment. Hence, the initial tether length was chosen to

be 10 times the final tether length and it was confirmed by numerical simulation that the target angular velocity will be reached under these conditions.

Assume that there is an event that causes the value of $\tilde{c}$ to be less than $\frac{3}{4}$. One such event is an an increase in tether reel-in time from 30 minutes to 60 minutes and this is the event that will be simulated. There are several plausible scenarios under which the reel-in time could increase in this manner. Two such scenarios are a decrease in tether reel-in system power or an unexpected increase in tether reel-in friction. It is also important to note that the same effect could be achieved without increasing the tether reel-in time. If, for instance, the final tether length L_f were increased, i.e. if the tether control system improperly sensed the tether length and the reel-in process discontinued before the desired L_f was reached, then $\tilde{c}$ would decrease. Also, a decrease in the initial tether length, which could occur if the tethered satellite were not deployed fully before the reel-in process started, could cause the value of $\tilde{c}$ to fall below $\frac{3}{4}$. Because the parameter $\tilde{c}$ incorporates all of the salient parameters of the planar dumbbell model, each of the above effects will affect the equations of motion in exactly the same way. As a result of the change in $\tilde{c}$ caused by the simulated increase in tether reel-in time, the maximum value of the x_2-nullcline is greater than the maximum value of the x_1-nullcline, i.e. the peak of the sinusoidal x_2-nullcline is greater than zero. If this happens, the sets comprising Regions 4, 6, 7, and 9 become non-empty. Tracing the tendencies of the solution trajectories using the rules previously stated, on the

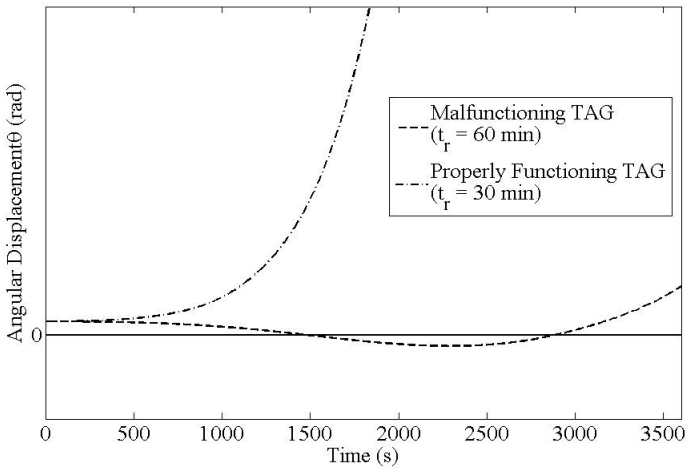

Figure 5.1: TAG malfunctioning solution trajectory in the θ, t plane. The malfunctioning trajectory does not increase in angular displacement as quickly as the functioning trajectory. Furthermore, the malfunctioning trajectory reaches maxima and minima (i.e., does not increase monotonically) in angular velocity, which can have undesired artificial gravity implications for a TAG system.

interval between the equilibria, the solution trajectories initially exist in Region 6 and immediately transition into Region 5. These trajectories cross the x_2-nullcline and circulate around the spiral equilibrium before entering a final constant spin in the positive x_2 direction. Physically, this corresponds to at least two changes in the sign of x_2 before the system enters its final spin. This is highlighted by examining a sample solution trajectory with initial x_1 value of approximately 0.75 radians. This solution trajectory in the $x_1 - t$ plane is shown in Fig.5.1. The path of one end-body in the orbital XY frame is shown in Fig.5.2. Compared to Fig.5.3, the end-body path shown in Fig.5.2 undergoes an oscillation in the sign of x_1 immediately before it

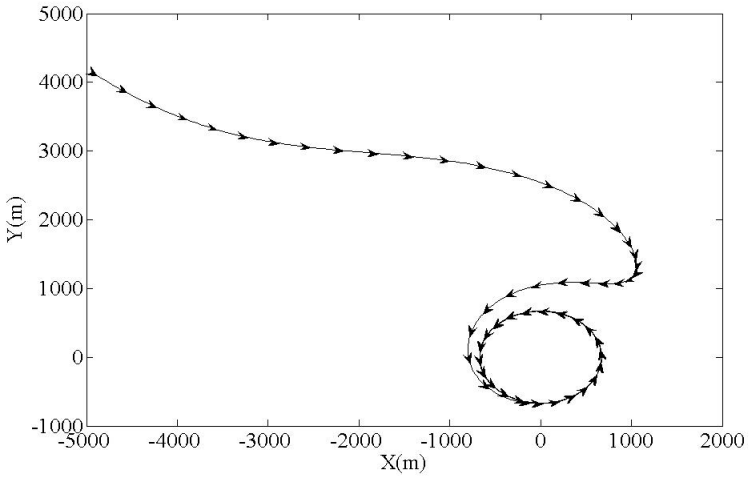

Figure 5.2: TAG end-body trajectory in the orbital plane, malfunctioning case. The arrows show the direction of the end-body at each point in time and are spaced equally in time.

enters its final spin. This"knee" in the plot causes the value of the artificial gravity felt by masses in the end-bodies to briefly fall to a very low value before the final spin is entered.

Solution trajectories with initial x_1 values close to the equilibria values evolve extremely slowly as t increases; this is shown in Fig.5.4. As t increases from 0 to the final reel-in time (3000 s), the trajectory only moves through a few hundredths of a radian. Solution trajectories that start some distance from the equilibria proceed to enter a spin-up regime much like the regime that occurs if $\tilde{c}$ is less than $\frac{3}{4}$. If the initial state of the system is not close to the equilibria in the phase plane, the system will freely enter a spin. This implies a design recommendation that the initial state of

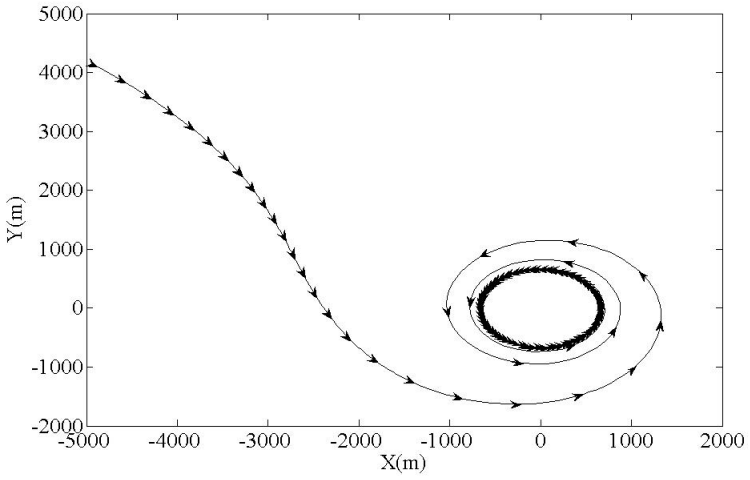

Figure 5.3: TAG end-body trajectory in the orbital plane, functioning case. The arrows along the path of the end-body show the direction of the local velocity and are spaced equally in time.

a tethered system be chosen so that it is not in the vicinity of the equilibria, and thus mission planners must be aware of the presence and location of the spiral equilibrium to avoid undesirable TAG behavior.

5.3 TAG Case Study 2: Martian Gravity Mission Design

The analysis previously set forth can be used to design a TAG mission to conform to a set of restrictions set forth by a mission planner. Conceivably, the mission planner will specify the final spin rate or artificial gravitational force of the system and the

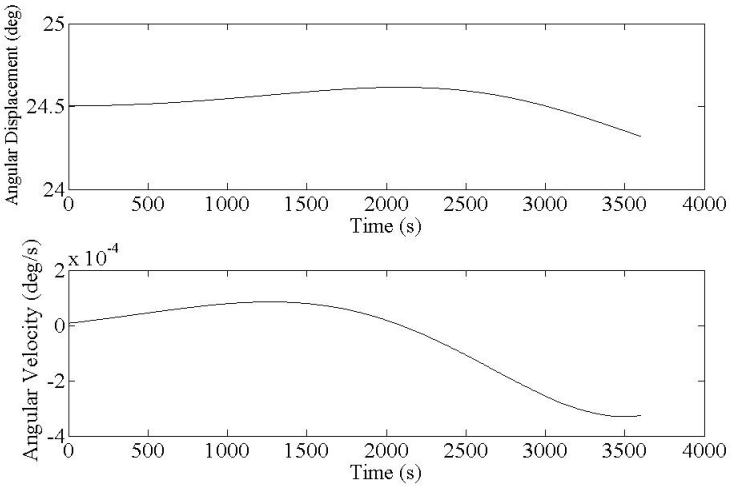

Figure 5.4: TAG malfunctioning solution trajectory near an equilibrium value. Note the small scale of angular displacement experienced over a large time and the low value of angular velocity attained during this simulation.

orbital radius of the center of mass of the system. The first assumption that can be made in TAG mission design is that the presence of equilibria in the system is not desirable; the absence of equilibria ensures that each of the solution trajectories will enter a final spin with a non-trivial angular velocity. In order to ensure that no equilibria are present, the value of the salient nondimensional parameter, $\tilde{c}$, of the system is restricted to be greater than $\frac{3}{4}$. According to the approximation for average steady state angular position and velocity (Eq.4.3), the value $\frac{L_i}{L_f}$ needed to obtain the angular velocity defined by the mission planner can also be calculated. Assume that the TAG mission to be designed is for a manned orbital station for which the artificial gravity imparted to bodies within the end masses is to be equal to $\frac{3}{8}g$ (i.e. equal to

the gravitational acceleration found on Mars). This type of TAG mission would be used to study the effects of martian gravitational accelerations on humans, plants, and materials and could be used as a precursor to a long term Martian base. Assume that the TAG system orbits at the same orbital radius (6878 km) indicated in previous sections. An angular rate of 1 rpm will ensure that humans do not feel discomfort due to Coriolis effects[41] and therefore $\dot{\theta} = 0.1047 rad/s, x_2 = 90.3365$, will be used to calculate the final tether length using Eq.5.2[39]. This length is approximately 671 meters.

Eq.4.6 indicates that an initial tether length of approximately 9.6 times the final tether length is necessary to achieve the desired final angular velocity. This indicates that the desired initial tether length is 2861 meters. This implies a tether reel-in time limit. Since $\tilde{c}$ must be greater than $\frac{3}{4}$, the following limit must be obeyed

$$\tilde{c} = \frac{ln\frac{L_i}{L_f}}{t_f \Omega} = \frac{ln 9.6}{t_f 0.0011069} = \frac{2043.3}{t_f} > \frac{3}{4} \tag{5.3}$$

which indicates that the tether reel-in time (t_f) must be less than 45.4 minutes. This limit, coupled with the fact that the tether length control law is to be exponential, gives criteria on which to base the tether reel-in system selection.

Assume that, to meet the restriction on tether reel-in time, a reel-in system which completes the reel-in process in 40 minutes is chosen; in this case $\tilde{c} = 0.8514$. At this point all physical parameters of the system have been chosen and the only other unknown values are the initial conditions. In order to choose appropriate initial

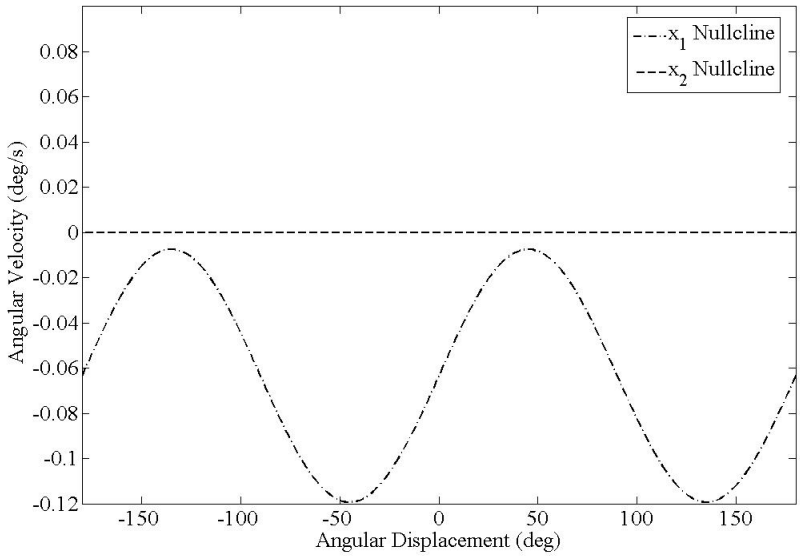

Figure 5.5: TAG malfunctioning solution trajectory near an equilibrium value. Note the small scale of angular displacement experienced over a large time and the low value of angular velocity attained during this simulation.

conditions, examine the plots of the nullclines in the phase plane. Fig.5.5 shows the nullclines on the phase plane. This figure shows that the x_2 (sinusoidal) nullcline reaches a maximum at approximately 0.25 radians (14.3 degrees) and a minimum at approximately -0.75 radians (-43 degrees). In order for the TAG system to reach a final spin-state with a minimum of changes in spin direction, it is best for the system to start in either Region 3 or Region 1, i.e. either on the x_1-nullcline (the abscissa) or above it. If this is the case, the solution trajectories begin near the nullclines and the system moves in a constant counterclockwise direction. As described earlier, the slope of the solution trajectories will be greatest at x_1 values for which the x_2 nullcline is

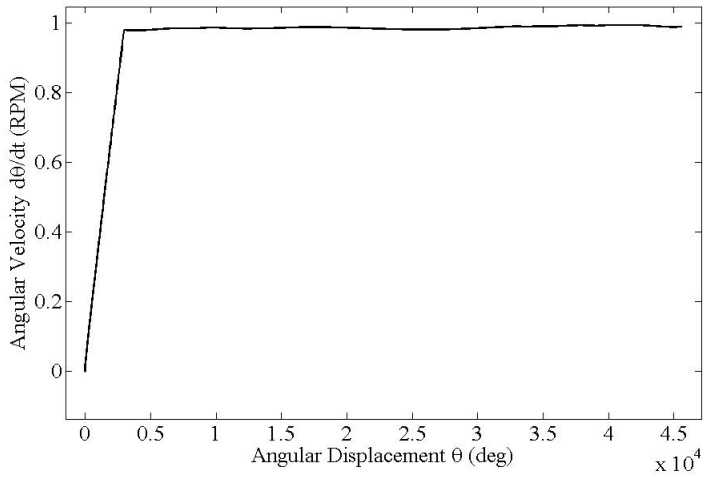

Figure 5.6: TAG Mission Design with the recommended initial θ value of -14.3 degrees (-0.25) radians shown. Note that the final angular velocity is very close to 1 rpm.

at a minimum. This indicates that as the x_1 value of the solution trajectories passes near the x_1 value for which the x_2-nullcline is least, the increase in angular speed with angular displacement is greatest. Therefore, the initial value of x_1 for the TAG system in question should be close to an x_1 value for which the x_2 nullcline is a minimum in order to ensure the quickest departure of the solution trajectory from the vicinity of the nullclines. This protects the solution trajectory from intersecting the nullclines and increases the likelihood that the solution trajectory behavior will be uniform as τ increases. Such an initial x_1 value is -14.3 degrees (-0.25 rad). The analysis above is further reinforced by the numerically generated graph (Fig.5.7) which shows that at an initial angular displacement of -0.25 radians, the final angular velocity is

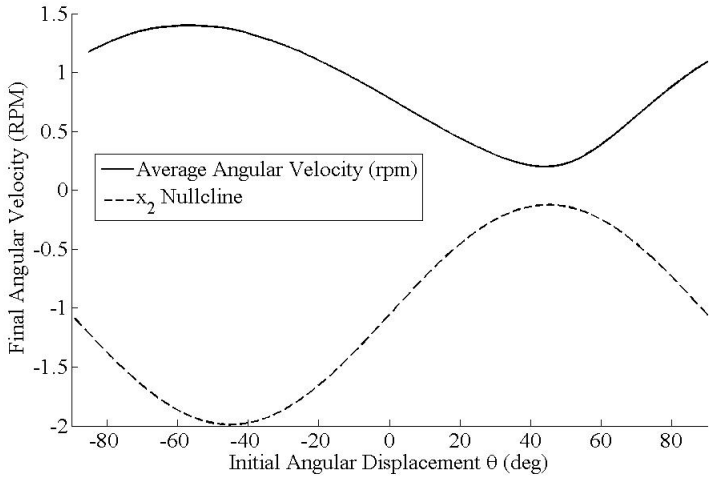

Figure 5.7: TAG Mission Design final $\dot{\theta}$ value versus initial θ. The value of the x_2 nullcline has been amplified by a factor of 100 in order to make the shape of the nullcline visible on the graph. Note the relationship between the maxima and minima of the two curves.

approximately 0.1044 rad/s. This is within 0.3% of the desired value. Fig.5.6 shows the behavior of a solution trajectory with an initial x_1 of -0.25 radians and an initial angular velocity of 0 rad/s.

An important aspect to mission design is the ability of the system to accomplish the task for which it was designed despite variations in the design parameters. Fig.5.7 suggests a one-to-one relationship between the initial angular displacement away from the local vertical and the final angular velocity reached by a TAG system. Therefore, any deviation in angular velocity would require a method, such as a thruster system, of either increasing or decreasing the angular rate of the TAG system in order to reach the target angular velocity. Such a system must be capable of injecting enough

angular momentum into the system to achieve the desired system angular velocity. Fig.5.7 suggests that in the lower end of the initial θ range, i.e. -60^o to -40^o, the final angular velocity is less susceptible to variations in the initial angular position. This corresponds to values x_1 for which the x_2-nullcline varies the most, i.e. where the value of the derivative $\frac{\partial x_2}{\partial x_1}$ is the greatest. As previously discussed in Section 4.2, the value of the derivative $\frac{\partial x_2}{\partial x_1}$ is greatest at values of x_1 for which the value of the x_2-nullcline is least. This generates a design recommendation that the initial x_1 value be chosen so that $\theta(t = 0)$ is an x_1 value for which the x_2 nullcline is a minimum. This ensures that the final angular velocity has the least dependence on the initial x_1 value, thus making the system more tolerant to variations in the initial value of x_1. This strategy would minimize the energy that would need to be expended in order to adjust the final angular velocity of the TAG system to the target final angular velocity.

The system will also have different behavior depending on the initial angular velocity of the system. As long as the initial angular velocity is in the positive θ direction (i.e., counterclockwise), the effect of the additional initial angular velocity can be seen by applying the approximation set forth for solution trajectories far from the nullclines. However, if the initial angular velocity is negative and lower in value than the maximum of the x_2-nullcline, the possibility for solution trajectory interaction with the x_2-nullcline exists. In order to prevent this interaction, an initial

angular displacement away from the local vertical that occurs at a relatively low value of the x_2-nullcline is desirable. If such an initial angular displacement is chosen, this reduces the chances that a solution trajectory will interact with the x_2-nullcline and produce undesirable dynamics.

A final type of potentially problematic behavior that could occur is mechanical malfunction in the reel-in system itself or possible orbital insertion into an orbit with a radius different than the design orbital radius. Either of these malfunctions would cause the value of $\tilde{c}$ to change. The most dramatic change in the dynamics of the system would occur if the value of $\tilde{c}$ were lowered so that the maximum of the x_2-nullcline approached the x_1-nullcline. If the value of $\tilde{c}$ reached or passed lower than the critical value of $\frac{3}{4}$, a bifurcation would occur in the system and equilibria would appear. These equilibria, as shown previously, have dramatic effects on the dynamics of TAG system behavior.

The existence of equilibria indicates that, under certain conditions, solution trajectories may circulate around the spiral equilibrium before they enter the spin-up stage. This is undesirable because of the oscillations in the magnitude of artificial gravity imparted to objects in the end-bodies during this circulation. Also, solution trajectories that pass sufficiently close to the equilibrium do not enter the spin-up stage during the tether reel-in period. This effect is shown in Fig.4.6. These trajectories indicate a physical system that oscillates like a pendulum rather than spinning

up. This regime is not useful for artificial gravity generation. It is possible to design a TAG mission that is not susceptible to these effects even for values of $\tilde{c}$ less than the critical value $\frac{3}{4}$. This can be accomplished with a wise choice of the initial system state. The solution trajectories most likely to be affected by changes in the value of $\tilde{c}$ are those which occur at x_1 values for which the x_2 value of the x_2-nullcline is greatest. Therefore, in order to minimize the effect of variations in $\tilde{c}$, an initial state should be chosen that occurs near x_1 values for which the x_2-nullcline value is least. These are states with initial angular displacements that are near -0.25 radians (-14.3 degrees) and initial angular velocities that are either positive or close to zero.

The nullclines of the Planar Dumbbell model can be used to determine the physical parameters of TAG satellites and, by using information regarding the possible initial conditions of the TAG satellite and the most likely failure mechanisms of the tether reel-in assembly, recommendations can be made regarding the initial states appropriate to increase the probability of a successful TAG mission. By studying variations in TAG system starting-states and physical parameters, there is one clear mission recommendation concerning the initial state of the tethered satellite system; namely initial states near x_1 values for which the x_2 nullcline is a minimum and x_2 values that are greater than or equal to zero are the ideal initial conditions for a TAG-type mission . The solution trajectories of systems with initial conditions which fit the above criteria will be less likely to intersect the x_2 nullcline than systems which

do not follow the above criteria. Avoiding intersections between solution trajectories and nullclines will result in physical systems for which θ increases with the minimum number of changes in the sign of $\dot{\theta}$; such uniform increase in θ results in uniform increase in the artificial gravity felt by masses inside a TAG satellite end-body. Tethered satellite solution trajectories with initial conditions that occur near x_1 values for which the x_2 value is a minimum also have the property that they move upward in the phase plane faster than other solution trajectories; this effect is discussed in Section 4.2 and is related to the fact that the local value of $\frac{\partial x_2}{\partial x_1}$ is a maximum at values of x_1 at which the x_2 nullcline is a minimum. For TAG satellites, solution trajectories that move faster in the x_2 direction achieve the artificial gravity level for which they were designed in a shorter amount of time. Choosing TAG initial conditions as described above also minimizes the effects on the solution dynamics of variations in the physical parameters of the system, expressed in the nondimensional constant $\tilde{c}$, and the initial velocity of the system. Changes in $\tilde{c}$ are manifested through a change in the proximity of the maximum of the x_2 nullcline to the x_1 nullcline. Therefore, to decrease the probability that a change in $\tilde{c}$ will generate equilibria near a potential solution trajectory, the initial conditions for the solution trajectory should be chosen so that they occur at x_1 values for which a minimum of the x_2 nullcline occurs. The nullclines of the Planar Dumbbell model can be used in this way to design TAG missions, and by using information regarding the possible initial conditions of the

TAG satellite and the most likely failure mechanisms of the tether reel-in assembly, recommendations can be made regarding the initial states appropriate to increase the probability of a successful TAG mission.

Chapter 6

Conclusion

Tethered satellite research began with the investigation of long bodies used to access space performed by Tsiolkovskii as early as 1895. Since that time, tethered satellites have been designed, flown, and analyzed by a host of people. Nullcline analysis, a tool developed through the study of ordinary differential equations, can be used to describe tethered satellite behavior under the planar dumbbell approximations with an exponential tether reel-in law. The equations of motion of the planar dumbbell model under an exponential reel-in law have been shown to contain one parameter $\tilde{c}$, which describes the physical parameters of the planar dumbbell tethered satellite. The effect of varying $\tilde{c}$ along with the effect of varying the initial conditions of the tethered satellite model have been studied using nullcline analysis. The character of the planar dumbbell solution trajectories through the phase plane can be understood in the context of the nullclines of the equations of motion. The utility of understanding

the character of the phase plane solution trajectories has been demonstrated using a Tethered Artificial Gravity (TAG) satellite as a canonical planar dumbbell system. The nullclines of the differential equations of a given TAG system can be used to determine the ideal mission initial conditions, determine the effect of changing TAG physical properties on the dynamics of the TAG satellite, and to determine the ideal TAG physical parameters. Each of these uses is of interest to planar dumbbell tethered satellite mission planners.

List of References

[1] Ivan Bekey. Historical evolution of tethers in space. In P.M. Bainum, I. Bekey, L. Guerriero, and P.A. Penzo, editors, *Tethers in Space: Proceedings of an Inernational Conference Held September 17-19, 1986, at Arlington, Virginia*, volume 62. American Astronautical Society, 1986.

[2] J.L. Synge. On the behaviour, according to newtonian theory, of a plumb line or pendulum attached to an artificial satellite. *Proceedings of the Royal Irish Academy, Section A (Mathematical, Astronomical and Physical Science)*, 60(1):1 – 6, 1959.

[3] Gemini Mission Evaluation Team. *Gemini XI Mission Report*. National Aeronautics and Space Administration Manned Spacecraft Center, Houston, Texas, 1966.

[4] Gemini Mission Evaluation Team. *Gemini XII Mission Report*. National Aeronautics and Space Administration Manned Spacecraft Center, Houston, Texas,

1967.

[5] A.K. Misra and V.J. Modi. A survey on the dynamics and control of tethered satellite systems. In P.M. Bainum, I. Bekey, L. Guerriero, and P.A. Penzo, editors, *Tethers in Space: Proceedings of an Inernational Conference Held September 17-19, 1986, at Arlington, Virginia*, volume 62. American Astronautical Society, 1986.

[6] G. Colombo, E. M. Gaposchkin, M. D. Grossi, and G. C. Weiffenbach. "sky-hook": A shuttle-borne tool for low altitude research. *Meccanica*, 10(1):3 – 20, 1975.

[7] M. D. Grossi and G. Colombo. Interactions of a Tethered Satellite System with the Ionosphere. In *Alabama Univ. UAH/NASA Workshop on the Use of a Tethered Satellite System p 177-181 (SEE N81-29479 20-42)*, pages 177–181, May 1978.

[8] M. Dobrowolny, G. Colombo, and M. D. Grossi. Electrodynamics of long conducting tethers in the near-earth environment. 1976.

[9] V. Chobotov. Gravity-gradient excitation of a rotating cable-counterweight space station in orbit. *Journal of Applied Mechanics*, pages 547–554, December 1963.

[10] V. Chobotov. Gravitational excitation of extensible dumbbell satellite. *Journal of Spacecraft and Rockets*, 4(10):1295 – 1300, 1967.

[11] C.L. Tai and M.M.H. Loh. Planar motion of rotating cable-connected space station in orbit. *Journal of Spacecraft and Rockets*, 2(6):889 – 894, 1965.

[12] C.D. Pengelley. Preliminary survey of dynamic stability of cable-connected spinning space station. *Journal of Spacecraft and Rockets*, 3(10):1456 – 1462, 1966.

[13] D.D. Nixon. Dynamics of a spinning space station with a counterweight connected by multiple cables. *Journal of Spacecraft and Rockets*, 9(12):896 – 902, 1972.

[14] F. Austin. Nonlinear dynamics of free-rotating flexibly connected double-mass space station. *Journal of Spacecraft and Rockets*, 2(6):901 – 906, 1965.

[15] V.V. Beletskii. Relative motion of a link-up of two objects in orbit. ii. *Kosmicheske Issledovaniya*, 7(6):827 – 40, 1969.

[16] R. B. Singh. Three-dimensional motion of a system of two cable-connected satellites in orbit. 18(5):301 – 308, 1973.

[17] G.G. Efimenko. Three-dimensional motion of two coupled bodies under the action of gravitational and aerodynamic forces. *Kosmicheske Issledovaniya*, 11(3):484 – 6, 1973.

[18] P.M. Bainum and K.S. Evans. Gravity-gradient effects on the motion of two rotating cable-connected bodies. *AIAA Journal*, 14(1):26–31, January 1976.

[19] P. M. Bainum and K. S. Evans. Three-dimensional motion and stability of two rotating cable connected bodies. *Journal of Spacecraft and Rockets*, 12(4):242 – 250, 1975.

[20] S.A. Crist and Eisley J.G. Cable motion of a spinning spring-mass system in orbit. *Journal of Spacecraft and Rockets*, 7(11):1352 – 7, 1970.

[21] W.P. Targoff. On the lateral vibration of rotating orbiting cables. *AIAA Journal*, 7(11):66–98, 1966.

[22] M. Ruiz and J. Pelaez. Slingshot orbital injection revisited. *Advances in the Astronautical Sciences*, 102(2):1381–1397, 1999.

[23] K.D. Kumar, T. Yasaka, and T. Sasaki. Orbit transfer of service vehicle/payload through tether retrieval. *Acta Astronautica*, 54(9):687 – 698, 2004.

[24] Paul A. Penzo and Harris L. Mayer. Tethers and asteroids for artificial gravity assist in the solar system. *Journal of Spacecraft and Rockets*, 23(1), 1984.

[25] E.C. Lorenzini, G.E. Gullahorn, and F. Fuligni. Recent developments in gravity gradiometry from the space-shuttle-borne tethered satellite system. *Journal of Applied Physics*, 63(1):216 – 23, 1988.

[26] Ernesto Vallerani and Franco Bevilacqua. New applications of tethered satellites: An italian perspective. In P.M. Bainum, I. Bekey, L. Guerriero, and P.A. Penzo, editors, *Tethers in Space: Proceedings of an Inernational Conference Held September 17-19, 1986, at Arlington, Virginia*, volume 62. American Astronautical Society, 1986.

[27] F.C. Hurlbut and J.L. Potter. Tethered aerothermodynamic research needs. *Journal of Spacecraft and Rockets*, 28(1):50 – 57, 1991.

[28] Monica Pasca and Enrico Lorenzini. Collection of martian atmospheric dust with a low altitude tethered probe. *Advances in the Astronautical Sciences*, 75(pt 2):1121 – 1139, 1991.

[29] Kurt A. Polzin, Edgar Y. Choueiri, Pini Gurfil, and N. Jeremy Kasdin. Plasma propulsion options for multiple terrestrial planet finder architectures. *Journal of Spacecraft and Rockets*, 39(3):347 – 356, 2002.

[30] V.J. Modi and R.P. Pidgeon. Dynamics and control of a flexible tethered system with offset. *Acta Astronautica*, 32(4):255 – 65, 1994.

[31] Marco B. Quadrelli. Dynamics and control of novel orbiting formations with internal dynamics. *Journal of the Astronautical Sciences*, 51(3):319 – 337, 2003.

[32] M.L. Cosmo and E.C. Lorenzini. *Tethers in Space Handbook*. NASA Marshall Space Flight Center, Huntsville, Al, 3rd edition, 1997.

[33] T.R. Kane. *Dynamics*. Holt, Reinhart, and Winston, New York, 1968.

[34] M.W. Hirsch, S. Smale, and R.L. Devaney. *Differential Equations, Dynamical Systems and An Introduction to Chaos*. Elsevier Academic Press, San Diego, 2nd edition, 2004.

[35] F. Brauer and J.A. Nohel. *The Qualitative Theory of Ordinary Differential Equations: An Introduction*. Dover Publications, New York, 1969.

[36] J.H. Hoffman and A.P Mazzoleni. Overview of the tag (tethered artificial gravity) satellite program. In *Proceedings of the 2002 AAS/AIAA Space Flight Mechanics Meeting, San Antonio Texas*. AAS/AIAA, January 2002.

[37] Bas Lansdorp, Michiel Kruijff, and Erik Jan V. D. Heide. The need for mars-g in leo: Manned antecedent for reduced and simulated gravity. *54th International Astronautical Congress of the International Astronautical Federation (IAF), the International Academy of Astronautics and the International Institute of Space Law*, 1:2111 – 2118, 2003.

[38] Carol Kowalsky and J. David Powell. Tethered artificial gravity spacecraft design. *Advances in the Astronautical Sciences*, 85(pt 1):645 – 664, 1993.

[39] B.M. Quadrelli and E.C. Lorenzini. Dynamics and stability of a tethered centrifuge in low earth orbit. *Journal of the Astronautical Sciences*, 40(1):3 – 25, 1992.

[40] Enrico C. Lorenzini. Three-mass tethered system for micro-g/variable-g applications. *Journal of Guidance, Control, and Dynamics*, 10(3):242 – 249, 1987.

[41] R.D. Reed and G.R. Coulter. Physiology of space flight. In W.J. Larson and L.K. Pranke, editors, *Human Spaceflight: Mission Analysis and Design*, Space Technology Series, chapter 5. The McGraw-Hill Companies, Inc., 1999.